Marine Pollution Bulletin 233 (2026) 120182

Contents lists available at ScienceDirect

Marine Pollution Bulletin

journal homepage: www.elsevier.com/locate/marpolbul

An integrated modeling framework for riverine macroplastic emissions, transport, and accumulation across the land-sea continuum

Ali Aalifar [a,b,*], William Mc Kiver [a], Christian Ferrarin [a], Francesca De Pascalis [a], Francesco Falcieri [a], Davide Zanchettin [b], Fantina Madricardo [a], Vanessa Moschino [a], Michol Ghezzo [a]

[a] Institute of Marine Sciences (ISMAR), National Research Council (CNR), Venice, Italy
[b] Department of Environmental Sciences, Informatics and Statistics, Ca' Foscari University of Venice, Venice, Italy

ARTICLE INFO

Keywords:
Riverine plastic emissions
Macroplastic pollution
Spatial probabilistic model
Hydrodynamic-Lagrangian modeling
River–sea systems

ABSTRACT

Plastic pollution in coastal environments is shaped by interactions among land-based emissions, river networks, and marine hydrodynamic processes, yet these processes are rarely examined within a unified approach. Here, we present an integrated source-to-sink modeling framework for macroplastic pollution across the river–sea continuum, coupling a spatial probabilistic model with the 3D SHYFEM hydrodynamic model and its Lagrangian particle-tracking module. Applied to the Venice Lagoon and adjacent northern Adriatic Sea, the framework quantifies how plastics are mobilized from land, transferred through river networks, and redistributed within coastal waters. The probabilistic component resolves spatiotemporal variability in riverine emissions by combining mismanaged plastic waste with meteorological, land-use, and hydrological drivers, while the hydrodynamic–Lagrangian component simulates transport pathways and accumulation patterns. Results show heterogeneous and seasonally variable riverine inputs, with baseline annual emissions of 4.23×10^4 kg yr^{-1}. The Brenta River contributed 37.3% of annual emissions, followed by the Sile (12.2%) and Dese (9.8%), while the top six rivers accounted for more than 80% of the total load. Source intensity strongly affected the magnitude and seasonal expansion of model-predicted potential accumulation zones, whereas their spatial distribution remained stable, indicating that hydrodynamic processes primarily controlled accumulation patterns. Simulated hotspot extent increased by 22% under the high-load case and decreased by 63% under the low-load case, although these model-predicted patterns require targeted field validation. The framework links inland emissions to coastal fate and supports the identification of key emission areas, transport pathways, and persistent accumulation zones to inform mitigation in river-dominated coastal systems.

1. Introduction

Plastic pollution is one of the most pervasive and persistent forms of anthropogenic contamination in aquatic environments. Estimates suggest that between 9.5 and 23 million metric tons of plastic enter aquatic systems each year (Borrelle et al., 2020; Cottom et al., 2024; Kaandorp et al., 2023; Lau et al., 2020). Plastic debris affects nearly all components of hydrological and ecological systems, from urban waterways and rivers to remote deep-sea environments (Canals et al., 2021; Gündoğdu et al., 2026; Koelmans et al., 2017; Thompson et al., 2024). Once in the water, plastics undergo a variety of physicochemical and biological transformations that alter their buoyancy, transport behavior, and eventual fate (Kaandorp et al., 2023; Koelmans et al., 2017). These transformations, such as fragmentation (Liro et al., 2025), coupled with local environmental conditions and hydrodynamic forcing, make plastic transport and accumulation a highly dynamic and nonlinear process. In addition to harming marine fauna through entanglement and ingestion, plastics disrupt benthic ecosystems, act as vectors for invasive species, and adsorb hazardous pollutants such as polychlorinated biphenyls (PCBs) and heavy metals, amplifying their ecological and human health impacts (Canals et al., 2021; González-Fernández et al., 2021; Hardesty et al., 2017).

Given these impacts, understanding the pathways of plastic transport from land to sea is critical, with rivers playing a central role in mediating this transfer. Global estimates suggest that rivers transport between 0.57 and 2.70 million metric tons of plastic debris annually, corresponding to

* Corresponding author at: Institute of Marine Sciences (ISMAR), National Research Council (CNR), Venice, Italy.
E-mail address: aliaalifar@cnr.it (A. Aalifar).

https://doi.org/10.1016/j.marpolbul.2026.120182
Received 4 May 2026; Received in revised form 21 July 2026; Accepted 21 July 2026
Available online 27 July 2026

12–40% of total ocean inputs (Gnann et al., 2026; Kaandorp et al., 2023; Lebreton et al., 2017; Meijer et al., 2021). However, substantial uncertainties in global riverine plastic export estimates mainly stem from diverse modeling approaches (González-Fernández et al., 2023; Roebroek et al., 2022). Roebroek et al. (2022) reviewed four main methods to estimate riverine plastic emissions: (i) temporal extrapolation, which directly scales short-term flux observations to yearly estimates but often misses extreme events; (ii) linear regression models that link plastic flux to environmental drivers (e.g., discharge, rainfall), where correlations can be weak and often non-linear; (iii) exponential regression models that combine discharge with mismanaged plastic waste (MPW), widely used for global estimates albeit reliant on uncertain MPW datasets (Cottom et al., 2024; Lebreton et al., 2017; Mai et al., 2020, 2023; Schmidt et al., 2017); and (iv) spatial probabilistic modeling, which accounts for land-use and distance to rivers but ignores temporal variability in plastic littering (Meijer et al., 2021). These modeling uncertainties are further exacerbated by fragmented monitoring: as highlighted by Hurley et al. (2023) and Haseler and Mihut (2026), the use of diverse sampling techniques, such as visual counts, nets, booms, unmanned aerial vehicles (UAVs), and waste collection, results in the capture of different plastic fractions. Quality assurance/quality control and consistent metadata reporting are therefore essential not only to improve comparability across studies but also to better constrain estimates of riverine plastic inputs and associated fluxes.

Beyond these sampling discrepancies, recent observational work shows that riverine plastic transport is far from linear. Hydrology strongly shapes variability, with floods dramatically increasing fluxes, accounting for about 30% of annual transport in just a few days, yet a significant part of mobilized plastics are retained on riverbanks and floodplains rather than exported downstream (Blettler et al., 2026; van Emmerik et al., 2023). Similarly, tidal dynamics and vegetation in rivers can create a stop–go transport cycle, with items spending almost half of their time trapped within the system (Corbau et al., 2026; Gallitelli and Scalici, 2024; Lotcheris et al., 2024; Schreyers et al., 2024).

Alongside these hydrological and geomorphological controls, anthropogenic drivers also play a decisive role in shaping macroplastic pollution in river systems. Studies in Ghana show that MPW is the strongest predictor of macroplastic pollution, while hydrological drivers are weak or inconsistent (Pinto et al., 2024). Evidence from Switzerland shows that macrolitter abundance is strongly linked to urban features, particularly roads and buildings, while forests and wetlands showed negative associations (Schreyers et al., 2024). At the global scale, recent estimates suggest around 0.5 Mt yr^{-1} of riverine plastic exports to the sea, with around 90% being macroplastic from diffuse waste in Asia, Africa, and South America, and 10% microplastics from wastewater in developed regions (Strokal et al., 2023).

After plastic debris enters coastal zones, specialized modeling approaches are essential to capture its fate within complex marine systems. Within semi-enclosed seas such as the Mediterranean and Adriatic, regional modeling has provided valuable insights into plastic transport, retention, and accumulation under realistic forcing conditions. In the Adriatic Sea, Liubartseva et al. (2016) highlighted the importance of riverine hotspots such as the Po River and Venice Lagoon, where coastal fluxes can reach 70 kg km^{-1} day^{-1} near the Po Delta. Hydrodynamic simulations by Ferrarin et al. (2021, 2024) and Aghito et al. (2023) further demonstrate how tides, winds, and frontal systems shape seasonal pathways and accumulation zones in the northern Adriatic. Observations corroborate that while much plastic is removed from surface waters, 70% or more of litter sinks to the seabed, where plastics comprise 60–80% of debris (Canals et al., 2021; Madricardo et al., 2020; Segur and Sonke, 2025). Kaandorp et al. (2020) estimated annual inputs into the Mediterranean at 2100–3400 tons, primarily from coastal populations (61%), rivers (32%), and fisheries (6%), and of all plastics introduced into the Mediterranean since 2006, an estimated 54% has accumulated on coastlines, 45% has sunk, and only 170–420 tons remain afloat, underscoring the importance of seabed interactions in fate modeling.

These dynamics are particularly pronounced in transitional environments, such as estuaries and coastal lagoons, where interactions among riverine inputs, tidal forcing, and human pressures govern the fate of plastic debris (Critchell and Lambrechts, 2016; Kaimathuruthy et al., 2025). Building on these regional insights, coastal lagoons, such as the Venice Lagoon, provide a paradigmatic example where the interplay of hydrodynamics, morphology, and anthropogenic pressures determines pollutant fate. The Venice Lagoon, the largest lagoon in the Mediterranean, is a shallow, semi-enclosed system strongly influenced by rivers, tides, wind, and human activities. Its geomorphology and hydrodynamics create highly variable transport and retention patterns. Cucco and Umgiesser (2015) showed, using a Trapping Index, that water residence times vary substantially across the lagoon, with tidal forcing generating long-term retention zones. Such variability suggests that plastics may become trapped in inner lagoon areas, delaying their export to the Adriatic Sea.

Local dynamics, driven by natural and anthropogenic factors, are further influenced by the overarching effects of climate change and regulatory interventions. Over the past three decades, relative sea level in the lagoon has risen by about 4.9 mm per year, while air and sea temperatures have increased by about 1.8 °C and 1.4 °C respectively (Ferrarin et al., 2024; Safaie et al., 2026; Zanchettin et al., 2021). Projections indicate that the frequency of extreme sea level events could rise significantly under sustained global warming, with the present-day 100-year event occurring up to ten times as frequently by 2050 under high-emission scenarios (Lionello et al., 2021b). The projected increase in high-water events implies more frequent activation of the Mo.S.E. (Experimental Electromechanical Module) barriers to prevent flooding (Lionello et al., 2021a); however, prolonged closure periods restrict water exchange and increase lagoon residence times. Together, these processes enhance hydrodynamic confinement and increase the likelihood of pollutant and plastic retention within the lagoon (Ferrarin et al., 2013). This retention is further enhanced by coastal ecosystems such as salt marshes, which act as natural sinks for particulate material (Puppin et al., 2024a, 2024b).

These vulnerabilities are consistent with field evidence showing widespread plastic contamination in the Venice Lagoon. Studies report significant microplastic concentrations in sediments and waters, with higher values in river-influenced areas and near urban centers (Cecchi et al., 2024; Cecchi and Poletto, 2025; Vianello et al., 2013). At the same time, riverine inputs are recognized as major drivers of lagoon water quality, delivering nutrients, contaminants, and particulate matter (Bonometto et al., 2019; Feola et al., 2024; Ostoich et al., 2018; Pesce et al., 2019). However, despite this evidence, plastic transport in the lagoon's tributary network remains virtually unexplored, leaving a critical gap in understanding how rivers shape plastic accumulation and export dynamics.

Addressing this gap requires modeling approaches capable of linking land-based inputs with transport and fate across transitional systems. Previous work has emphasized that realistic simulations of plastic behavior demand more than simple surface advection (De Groodt et al., 2026). Madricardo et al. (2020) argued that comparisons with field data are only meaningful when based on high-resolution 3D hydrodynamic models coupled with particle tracking that explicitly accounts for wind drift, particle sinking, and near-bottom transport. A crucial uncertainty, however, lies in defining the model inputs in terms of frequency, quantity, and type of litter entering the system (Wickramarachchi et al., 2025).

The land–sea continuum, spanning from terrestrial landscapes to marine waters, is typically investigated through fragmented disciplinary approaches, with river basin modeling and marine hydrodynamics treated as separate domains (Pascalis et al., 2025). As highlighted by Van Sebille et al. (2020) and Maximenko et al. (2019), there is a growing need for integrated modeling frameworks that connect plastic emission estimates with downstream transport and fate processes. Recent advances in plastic emission modeling offer a promising way forward. Spatial probabilistic models, such as that developed by Meijer et al. (2021), combine MPW datasets, terrestrial features, hydrological data, and atmospheric drivers (e.g., rainfall and wind) to estimate plastic loads entering rivers. These models provide spatially resolved plastic input estimates but are rarely coupled with hydrodynamic and Lagrangian particle-tracking models that resolve downstream transport processes. A limited number of studies have begun to link emission estimates with particle tracking in coastal and semi-enclosed systems, including applications in the Mediterranean (Weiss et al., 2025) and the Black Sea (Zlateva et al., 2024). However, these approaches typically rely on simplified source representations or prescribe inputs at river mouths, without explicitly resolving the spatial heterogeneity and temporal variability of land-based emissions. A key knowledge gap therefore remains in linking spatially and temporally variable land-based plastic emissions with hydrodynamic transport, retention, and export in transitional river–sea systems. Bridging these approaches is essential for capturing both emission patterns and downstream transport dynamics.

The present study addresses this challenge by developing an integrated modeling framework for macroplastic transport and accumulation across a connected river–sea system, using the Venice Lagoon and the northern Adriatic Sea as a case study to evaluate the framework. This area is particularly well suited for such analysis because of its dense population, diverse land use, hydrological complexity, and ecological sensitivity. Moreover, it features multiple rivers discharging into a semi-enclosed lagoon before reaching the Adriatic Sea, creating a natural laboratory for investigating plastic dynamics along the land–sea continuum. The novelty of this study lies in coupling spatially resolved estimates of monthly riverine plastic emissions with a hydrodynamic–Lagrangian particle-tracking model, allowing plastic sources, transport pathways, retention zones, and export toward the sea to be analyzed within a single framework. The specific aims are to: (i) estimate the spatial and temporal variability of riverine macroplastic inputs to the Venice Lagoon; (ii) simulate the transport, retention, and export of river-derived macroplastic under realistic hydrodynamic forcing; and (iii) assess how contrasting plastic emission scenarios influence potential accumulation patterns across the river–lagoon–sea continuum. We hypothesize that riverine macroplastic inputs are spatially and temporally uneven, with a limited number of tributaries and months contributing disproportionately to total emissions. We further hypothesize that the formation of model-predicted potential accumulation zones is governed not only by input magnitude, but also by hydrodynamic conditions, including circulation patterns and residence time, while contrasting emission scenarios mainly affect the intensity rather than the spatial structure of accumulation.

2. Materials and methods

2.1. Integrated modeling framework

This study employs an integrated modeling framework that couples a spatial probabilistic emission model with a hydrodynamic–Lagrangian model to simulate plastic transport pathways, enabling a continuous representation of plastic dynamics across the land–sea continuum. The first component quantifies plastic loads entering the river–coastal system based on MPW, hydrometeorological conditions, and terrestrial characteristics. The second component simulates the subsequent transport, retention, and export of plastics using hydrodynamic fields and a Lagrangian particle-tracking model. Together, these components establish a source-to-sink linkage that captures both terrestrial emissions and marine dispersal under realistic environmental forcing. The overall workflow of the integrated framework is illustrated schematically in Fig. 1.

2.1.1. Spatial probabilistic modeling of riverine plastic emissions

The spatial probabilistic model (SPM) quantifies the fraction of MPW generated on land that is mobilized, moved to river networks, and

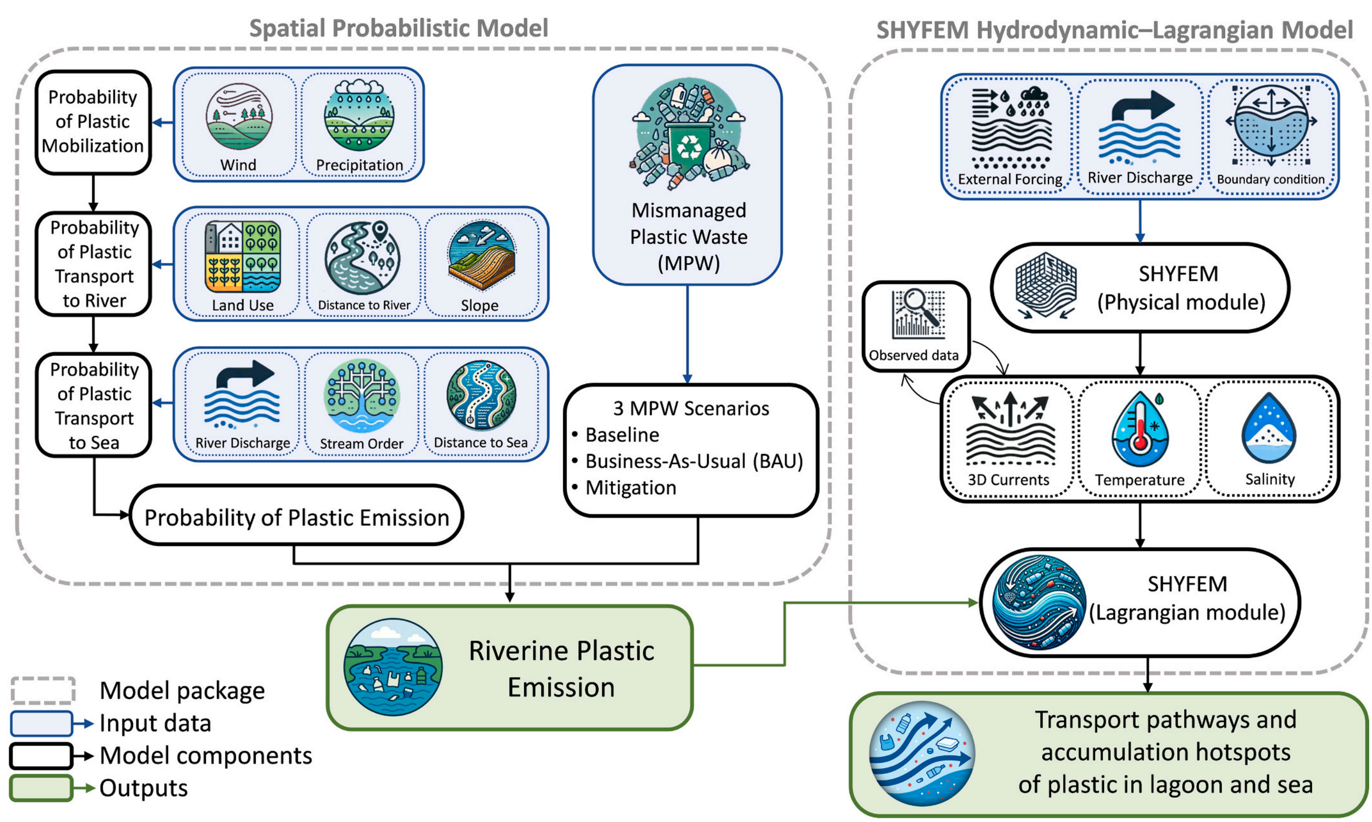

Fig. 1. Conceptual framework of the spatial probabilistic model and the Hydrodynamic-Lagrangian Model.

ultimately discharged into coastal waters. The approach adapts the probabilistic framework proposed by Meijer et al. (2021), in which the total emission probability ($P_{(E)}$) is defined as the product of three probabilities: the probability of mobilization on land ($P_{(M)}$), the probability of transport to the river network ($P_{(R)}$), and the probability of transport from the river to the sea ($P_{(O)}$). This formulation provides a flexible and transferable framework for representing plastic emission processes across regions with varying environmental and data conditions.

Mobilization probability is parameterized as a function of precipitation and wind intensity, which act as the primary drivers of plastic entrainment from the land surface. The probability of reaching a river depends on terrain slope, land-use roughness, and downslope distance to the nearest river, capturing the influence of topography and surface characteristics on overland transport. The probability of plastic transport to the sea increases with river discharge and stream order but decreases with distance from the outlet. For each grid cell, the three component probabilities are combined to calculate the total emission probability.

The mass of plastic entering the coastal environment ($M_{(E)}$) is estimated by combining basin-scale MPW generation with the spatially averaged emission probability, thereby linking land-based sources to riverine export. Time-varying emissions are obtained by aggregating these fluxes across river basins. While the probabilistic formulation follows Meijer et al. (2021), the estimation of emissions is adapted in this study to account for basin-scale aggregation and monthly variability in emission fluxes. All equations and parameterizations are provided in Eqs. (S1)–(S5) and Table S1 of the Supplementary Material (SM).

2.1.2. Hydrodynamic–Lagrangian modeling of marine plastics

Hydrodynamic transport is simulated using the three-dimensional finite-element model SHYFEM (System of HydrodYnamic Finite Element Modules, https://github.com/shyfemcm), which solves the primitive equations on unstructured triangular meshes. The model employs a semi-implicit time integration that is unconditionally stable for gravity waves, bottom friction, and Coriolis terms while treating advection explicitly. Water levels are computed at nodes and velocities at element centers in the horizontal dimension, and a flexible Z-layer discretization is used in the vertical dimension (Arpaia et al., 2023). Extensive descriptions of the numerical formulation and previous applications are available in Umgiesser et al. (2004) and Ferrarin et al. (2017, 2019).

Plastic transport is represented with an offline 3D Lagrangian particle tracker driven by SHYFEM hydrodynamic outputs. Particle positions are advanced with the resolved Eulerian velocities and a stochastic random-walk component that reflects subgrid turbulent diffusion. Wind effects on buoyant, near-surface debris are included through a parameterized Stokes drift acting on surface particles. Particles can sink with a constant settling velocity and may beach at the coastline; interactions with the bed allow either deposition or near-bottom transport depending on local conditions.

Previous applications of SHYFEM in the Venice Lagoon and Adriatic Sea support its suitability for resolving hydrodynamic and transport processes in complex coastal and lagoon environments (Bajo et al., 2023; Ferrarin et al., 2019, 2024, 2025; Lagomarsino-Oneto et al., 2024; Umgiesser et al., 2022).

2.2. Study area and model configuration

2.2.1. Site description

The Venice Lagoon, located in the northwestern Adriatic Sea (Fig. 2), is the largest coastal lagoon in the Mediterranean, covering an area of approximately 550 km^2. It is a shallow, microtidal system characterized by a semidiurnal tidal regime with a mean tidal range of 1.0 m and an average depth of 1.5 m. The lagoon is connected to the Adriatic Sea through three tidal inlets, Lido, Malamocco, and Chioggia, that together regulate tidal exchange and drive lagoonal circulation (Ferrarin et al., 2013). These inlets divide the lagoon into three hydrodynamic subbasins, each comprising a network of main and secondary channels that branch into smaller tidal creeks and salt marshes. The bathymetry is highly variable, ranging from intertidal salt-marsh flats (<0.5 m) to deep channels exceeding 15 m; with localized scour holes reaching depths of 40–50 m (Madricardo et al., 2019, 2021).

Freshwater inputs originate from 11 main tributaries distributed

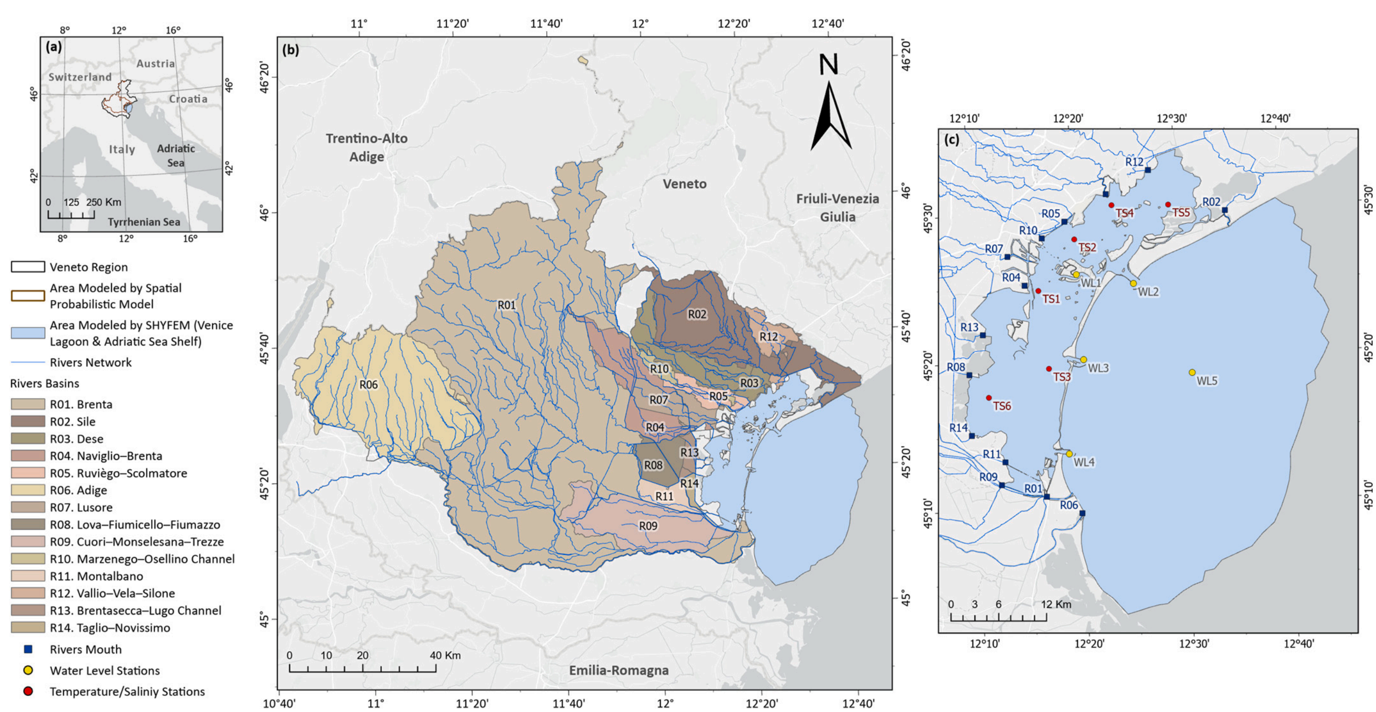

Fig. 2. Map of the case study area showing the river basins draining into the Venice Lagoon within the Veneto region (northeastern Italy), together with the lagoon, the locations of river mouths, and the observational stations for temperature, salinity, and water level.

along the inner lagoon boundary (Çevirgen et al., 2020; Zuliani et al., 2005). The drainage area of the tributaries directly connected to the Venice Lagoon covers approximately 1807.33 km^2 and is located in the Veneto Region, encompassing diverse terrain, including plains, hills, and mountainous areas. In contrast, the cumulative contributing area considered in the riverine plastic-emission model is 8471.81 km^2, as it includes the full contributing basins of the Brenta, Adige, and Sile river systems. Land use across the region ranges from densely populated urban and industrial areas to agricultural zones and natural reserves. Submarine groundwater discharge also contributes significantly to the freshwater budget, estimated to range between 15% and 80% of the total inflow (Zirino et al., 2016). As a result, salinity in the lagoon varies from around 20 PSU in the northern freshwater-influenced zones to 35 PSU near the inlets. Water residence times are spatially heterogeneous, from 1 to 3 days near the inlets to 15–20 days in the inner lagoon (Cucco et al., 2009).

The lagoon is strongly affected by meteorological forcing. North-easterly Bora winds generate strong currents and waves, while south-easterly Sirocco winds drive storm surges and coastal flooding (Tommasini et al., 2019). The system is further shaped by long-term human interventions. River diversions since the 16th century reduced sediment supply, promoting erosion and deepening of the lagoon (Bondesan, 2017; Puppin et al., 2024a, 2024b). More recent engineering works, including the excavation of navigation channels and the construction of the Mo.S.E. flood-barrier system, have further altered hydrodynamics, sediment transport, and salt-marsh sedimentation (Mel et al., 2021; Tognin et al., 2021). By 2002, the salt-marsh area had declined from around 180 km^2 in 1811 to 43 km^2 (Carniello et al., 2009), significantly reducing the lagoon's natural buffering capacity against sea-level rise.

The Venice Lagoon and the adjacent Gulf of Venice are among the most anthropogenically impacted coastal systems in Europe. Urbanization, port activities, intensive fishing and aquaculture, and heavy marine traffic exert strong pressures on water quality and sediment dynamics (Micheletti et al., 2011). Freshwater inputs from the surrounding drainage basins, characterized by extensive agriculture and industry, deliver nutrients, contaminants, and floating litter into the lagoon, while wind- and tide-driven exchanges redistribute pollutants toward the northern Adriatic. The combination of complex hydrodynamics, diverse land uses, and multiple sources of anthropogenic stress makes the Venice Lagoon an ideal natural laboratory for studying macroplastic transport and accumulation processes across the river–sea continuum.

2.2.2. *Configuration of the plastic emission model*

In this study, the SPM was refined and adapted to the Veneto region by introducing two key improvements: an increase in spatial resolution to a 10 m × 10 m grid and the incorporation of a monthly temporal resolution for the year 2019. This enhancement allows the model to resolve finer-scale spatial variability and seasonal dynamics associated with rainfall, wind, and river water discharge. The emission probability of each grid cell is thus determined by its terrestrial, hydrological, and anthropogenic characteristics, which jointly control the mobilization of plastics across the land–sea continuum. Since the analysis is limited to the Veneto portion of the domain, only the contribution of the Adige River's lower basin within Veneto was considered.

The model integrates environmental, hydrological, and MPW variables to estimate plastic mobilization and transport probabilities at high spatial and temporal resolution. Terrain slope and flow direction were derived from the TINITALY digital elevation model (Tarquini et al., 2007). These parameters were used to compute the downslope distance from each grid cell to the nearest river, defining overland connectivity for plastic transport. Monthly precipitation and wind speed for 2019 were obtained from the Regional Agency for Environmental Prevention and Protection of Veneto (ARPAV), based on observations from 196 meteorological stations. The data were spatially interpolated over the 10 m grid and used to represent the mobilization drivers in $P_{(M)}$.

River discharge data were compiled from ARPAV gauging stations. For rivers lacking direct measurements, discharge was estimated from CERRA-Land sub-daily regional reanalysis runoff data (Verrelle et al., 2022) and converted to monthly means. The river network and basin boundaries were obtained from ARPAV's Hydrographic Graph (ARPAV, 2022a) and Detailed River Basins (ARPAV, 2022b) datasets. Land-use information was derived from the Veneto Region Land Cover Map Database (Regione del Veneto, 2022). Each land-use category was assigned a roughness coefficient following Meijer et al. (2021) to represent its relative capacity to facilitate or impede plastic transport. Urban surfaces, for instance, were assigned higher transport probabilities, while forests and wetlands were assigned lower values (Table S2).

Population data used to scale MPW generation were obtained from the Italian National Institute of Statistics (ISTAT, 2021) for the total population of Italy in 2019, and from the Veneto Regional Statistical Office (SISTAR) for the resident and tourist populations of each municipality (SISTAR, 2025). Administrative boundaries of the municipalities were extracted from the Veneto Region's "Polygonal Administrative Boundaries of Municipalities" dataset (Regione del Veneto, 2024). The total population for each municipality was defined as the sum of the resident population and average tourist presence, the latter estimated from monthly tourist presences divided by the number of days in each month.

The estimation of monthly MPW under different source-intensity sensitivity scenarios followed a two-step procedure. First, annual MPW values for Italy were adopted from Lebreton and Andrady (2019) under contrasting assumptions of plastic production and waste management. These include a baseline-load condition for the 2019 reference year, a high-load source-intensity case based on the Business-as-Usual assumption of Lebreton and Andrady (2019), and a low-load source-intensity case based on their Mitigation assumption. These scenarios are not intended as explicit temporal projections, nor as predictions of future socio-environmental or policy trajectories, but rather as controlled sensitivity cases used to isolate the effect of varying riverine plastic source intensity under identical hydrodynamic and meteorological forcing. Second, annual MPW was converted into monthly per-capita values by dividing by 12 months and the national population of Italy for the 2019 reference year. These values were then scaled to each municipality according to its total population. Finally, the spatial intersection between municipal boundaries and river basins was used to allocate monthly MPW to each basin draining into the Venice Lagoon, preserving the spatial heterogeneity of population-driven plastic emissions.

To evaluate the influence of parameter choices on the SPM, a local one-at-a-time (OAT) sensitivity analysis was performed for two representative river basins, the Brenta and Dese. These rivers were selected because they represent important freshwater and plastic inputs to the Venice Lagoon system and differ in basin size and hydrological characteristics. Each parameter controlling plastic mobilization, overland transport, and riverine transport was individually perturbed while all other parameters were kept fixed at the reference configuration. Lower-bound simulations used parameter values divided by 10, whereas upper-bound simulations used values multiplied by 10, with probability-threshold parameters capped at 1 where applicable. The tested parameters were the precipitation coefficient (α), wind coefficient (β), slope threshold (τ), stream-order coefficient (θ), stream-order lower threshold (ι), discharge coefficient (κ), discharge lower threshold (μ), and land-use coefficient (ν). The complete set of OAT parameter values is reported in Table S3. Since independent macroplastic emission observations were not available, the sensitivity analysis was evaluated relative to the baseline configuration rather than against field observations. Sensitivity was expressed as the ratio of annual emissions in each sensitivity simulation to those in the baseline simulation, $M_{E,\text{sensitivity}}/M_{E,\text{baseline}}$, together with its logarithmic response, $\log_{10}(M_{E,\text{sensitivity}}/M_{E,\text{baseline}})$.

Based on the initial OAT screening for the Brenta and Dese basins, the five most influential parameters were further evaluated across all river basins. Each parameter was varied individually by −50% and +50% relative to its baseline value, while all other parameters were held constant; upper values of probability parameters were capped at 1. For each configuration, annual emissions were recalculated for every river, and changes in total regional emissions and river rankings were evaluated relative to the baseline.

To assess hydrometeorological controls on seasonal emissions, Spearman rank correlations were calculated between monthly macroplastic emissions and basin-averaged precipitation, wind speed, and river discharge for the Brenta and Dese basins. The correlations are interpreted as measures of seasonal co-variation rather than independent causal contributions. The detailed equation is provided in the Supplementary Material (Eq. (S6)).

To better understand how short-term hydrological variability may influence emission estimates that are otherwise based on monthly averages, we conducted a daily-resolution sensitivity analysis. In this analysis, emission probabilities were recalculated by varying only river discharge at daily resolution, while keeping other predictors unchanged. Precipitation and wind were not included at daily resolution because consistent, spatially resolved datasets for these variables were not available for the study period. Daily values of $P_{(O)}$ and consequently $P_{(E)}$ were computed based on observed discharge for Brenta and Dese in November 2019. This month was selected since it exhibited pronounced discharge variability, including distinct high-flow events, making it a representative period to assess the influence of short-term hydrological fluctuations. The resulting daily $P_{(E)}$ values were then averaged and multiplied by the daily MPW to estimate M_E. This approach captures the influence of discharge variability on emission probabilities and resulting emissions without altering the underlying monthly MPW input.

2.2.3. SHYFEM hydrodynamic and particle tracking configuration

The computational domain covers the entire Venice Lagoon together with the adjacent northern Adriatic shelf. The unstructured grid contains 17,515 nodes and 32,207 elements. The water column is divided into 18 Z-layers with thicknesses ranging from 0.5 m near the surface to 20 m at depth, allowing the model to resolve tidal propagation across shallow flats and vertical shear in tidal channels. The unstructured grid, together with lagoon bathymetry, is shown in Fig. S1.

Bathymetry was assembled from datasets covering the Venice Lagoon and the northern Adriatic Sea. Bathymetry for the Venice Lagoon was derived from datasets collected between 1999 and 2003, covering the entire lagoon including shallow areas, and from channel network surveys conducted in 2013 (Gavazzi et al., 2016). For the adjacent Adriatic Sea, bathymetric data were obtained from the EMODnet Bathymetry dataset, complemented by inlet surveys (Madricardo et al., 2017) and the CNR-ISMAR Adriatic survey (Foglini et al., 2012). All data were interpolated onto the triangular mesh with a common vertical datum. The model includes wetting and drying so that intertidal marshes and very shallow flats can intermittently emerge and flood during the tidal cycle. The simulation spans calendar year 2019, preceded by a spin-up period during December 2018 to stabilize water levels, density fields, and residual circulation before analysis. Meteorological forcing fields consisted of time series of wind, precipitation, and heat fluxes measured at the Acqua Alta platform. These fields were mapped onto the unstructured ocean grid at each hydrodynamic time step.

Freshwater inputs to the model domain include both rivers directly discharging into the Venice Lagoon and major rivers entering the adjacent Adriatic shelf. A total of 11 tributaries flow directly into the Venice Lagoon, for which time series were compiled from gauging stations where available; for ungauged tributaries, water discharges were derived from the CERRA-Land regional reanalysis. In addition, three major rivers located along the lagoon boundaries are considered: the Brenta and Sile rivers, which split into two branches, with one branch discharging into the lagoon and the other into the Adriatic Sea, and the Adige, which discharges entirely into the Adriatic Sea outside the lagoon system. Their mean annual discharges are 140.01 $m^3\ s^{-1}$ (Brenta), 54.35 $m^3\ s^{-1}$ (Sile), and 226.53 $m^3\ s^{-1}$ (Adige), substantially higher than the mean discharge of the Venetian tributaries (4.98 $m^3\ s^{-1}$). Freshwater salinity at river boundaries is set to near-zero values unless observations are available; river temperatures follow basin conditions or are gradually adjusted to modeled ambient values.

Open-sea boundary conditions include tidal elevations, depth-varying currents measured at the Acqua Alta platform (15 km offshore), and temperature and salinity fields obtained from the Copernicus Marine Service (Escudier et al., 2021). These datasets are used to impose both tidal forcing and baroclinic conditions at the open boundary, ensuring consistency between shelf-scale dynamics and lagoon exchange.

Monthly river-borne macroplastic loads produced by the spatial probabilistic model are converted from mass to items using a mean mass per item of 0.019 kg $item^{-1}$ (Meijer et al., 2021). For each river and month, the corresponding number of items is released at the river mouth elements and distributed uniformly in time within the month. Particles are released at the surface; during transport, they are subject to wind drift, horizontal and vertical diffusion, and a constant settling velocity of 1×10^{-4} m s^{-1}, consistent with MAELSTROM 2023 sensitivity tests, which indicate a settling time of approximately 5 days through a 40 m water column. The particle tracking model time step is 10 s, ensuring accurate resolution of advection between element faces and across vertical interfaces.

To assess the sensitivity of the simulated accumulation patterns to the assumed particle settling behavior, two additional Lagrangian simulations were performed using settling velocities of 1×10^{-5} and 1×10^{-3} m s^{-1}. These were compared with the baseline value of 1×10^{-4} m s^{-1}. The sensitivity test was conducted for four representative months, January, May, August, and November. These four months were not intended to reproduce the full annual variability, but to provide a representative seasonal sample for testing whether the predicted accumulation patterns and vertical partitioning were sensitive to the prescribed settling velocity. Details of the metrics used for the settling-velocity sensitivity analysis are provided in the Supplementary Material (Eqs. (S7)–(S10)).

The particle-tracking framework can represent sinking, shoreline interaction, and near-bottom transport. In the present configuration, particle behavior was simplified using a prescribed settling velocity, without dynamically representing changes caused by biofouling, fragmentation, or degradation. Explicit permanent shoreline beaching was not activated since preliminary tests indicated strong grid-dependent trapping near some river-mouth release locations. The model nevertheless accounts for wetting and drying of shallow and intertidal elements, so particles may be temporarily immobilized when an element becomes dry and resume transport after rewetting.

Three source-intensity sensitivity scenarios were simulated under identical hydrodynamic and meteorological conditions to isolate the effect of source intensity. These include a baseline condition for 2019, a high-load source-intensity case, and a low-load source-intensity case. This experimental design allows isolating the effect of source intensity on plastic transport pathways, retention within the lagoon, and export to the coastal sea, thereby enabling a controlled sensitivity analysis of the system response to variations in emission magnitude alone.

To evaluate the performance of the hydrodynamic model, statistical comparisons were carried out between simulated and observed values of water level, salinity, and temperature. Observations of water level were available for five stations distributed across the system, one near the main Venice Island, three at the lagoon inlets (Lido, Malamocco, and Chioggia), and one located offshore in the Adriatic Sea. The records cover the entire year 2019 with an average sampling interval of 15 min (Venice Municipality tidal network). For salinity and temperature, data from six monitoring locations were used (SAMAnet network), based on field samples collected throughout 2019 at an average temporal resolution of 1 h. The geographical locations of all stations and sampling sites are shown in Fig. 2.

The model performance was assessed using four statistical indicators: Pearson correlation coefficient (R), centered root mean square error (CRMSE), the difference between the mean of the model results and of the observations (BIAS), and the RMSE–observations standard deviation ratio (RSR). These metrics quantify the accuracy, systematic deviation, and overall skill of the simulations in reproducing observed hydrodynamic variables. All indices were calculated following standard formulations (Willmott, 1981, 1982), as reported in the SM (Eqs. (S11)–(S14)).

The detailed evaluation of model performance is provided in the SM (Section S4; Table S4; Figs. S2–S7). In summary, the hydrodynamic model reproduced water level and temperature with high accuracy across all stations, with correlation coefficients generally exceeding 0.9, while salinity was simulated with lower skill and larger spatial variability. Overall, the model successfully captured the main temporal dynamics and seasonal variability of the system, providing a reliable representation of the hydrodynamic conditions driving particle transport. These results are consistent with previous applications of the SHYFEM modeling framework in the Venice Lagoon and other coastal systems, where high performance has been reported for water levels, temperature, and salinity (Umgiesser et al., 2014, 2016, 2022). This consistency supports the robustness of the model and its suitability for investigating transport and accumulation processes in river–coastal systems.

To further assess the plausibility of the simulated Lagrangian transport pathways, an observational comparison was performed using GPS-tracker trajectories obtained from the WebGIS of the MISP project, "Misure sperimentali nei corsi d'acqua del Distretto Alpi Orientali per la cattura dei rifiuti galleggianti" (Autorità di bacino distrettuale delle Alpi Orientali, 2026). The MISP project is coordinated by the "Autorità di bacino distrettuale delle Alpi Orientali", with Veritas and "Consorzio di bonifica Acque Risorgive" as implementing partners. The dataset used here consists of floating GPS trackers released at different locations in the lagoon, with recorded release positions, time-stamped trajectories, and final observed positions. In total, 21 GPS-tracker trajectories were selected for this comparison based on whether their release points were located within or close to the model domain. For each observed tracker, an ensemble of 200 particles was initialized within a 200 m radius of the corresponding tracker release location, using the same particle-tracking configuration adopted in the main simulations, except that particles were treated as surface-floating tracers with no settling velocity.

This comparison should be interpreted as a semi-quantitative observational consistency check rather than a formal validation. The main hydrodynamic simulation used in this study refers to 2019, whereas the available GPS-tracker deployments were carried out in 2025. Therefore, the observed and simulated trajectories were not forced by the same meteorological and hydrodynamic conditions. To make the comparison more physically consistent, the model release times were selected using a tidal-analogue approach rather than by simply preserving the same calendar dates. Specifically, release dates in the same month of 2019 were selected to reproduce tidal conditions comparable to those observed during the GPS deployments, since tidal forcing is a dominant driver of short-term transport in the Venice Lagoon (Ferrarin et al., 2024; Umgiesser et al., 2004). The comparison was then performed using elapsed time after release, and simulated and observed positions were compared at matched elapsed times. Details of the comparison procedure are provided in the SM, including the selected observed and model release dates, the observed and simulated trajectory map (Fig. S8), the metrics table (Table S5), and the equations used to calculate the comparison metrics (Eqs. (S15)–(S22)), including nearest-particle RMSE and trajectory skill scores.

Despite the temporal mismatch between the GPS deployments and the hydrodynamic simulation year, several cases showed encouraging agreement between observed and simulated transport pathways. For instance, tracker ID 13 showed a nearest-particle RMSE of 0.12 km and a nearest-particle skill score of 0.96. Across the 21 analyzed trajectories, the mean nearest-particle RMSE was 1.28 km, while the mean nearest-particle skill score was 0.50 (Table S5). These results indicate that, although the comparison cannot be considered a strict validation, the particle-tracking framework can reproduce several observed transport pathways at the lagoon scale.

Model-predicted potential accumulation zones were identified from the gridded particle density fields derived from the Lagrangian simulations. Particle density was expressed as items per square meter (items m^{-2}) on a structured grid with a horizontal resolution of approximately 78 m × 111 m. A threshold-based approach was adopted, where grid cells with particle densities equal to or greater than 10 items m^{-2} were classified as simulated hotspots. This threshold was selected as an operational criterion to distinguish significant accumulation zones from background concentrations while ensuring consistency across scenarios. Given the absence of a universally accepted definition of plastic pollution hotspots, threshold values are often defined in a context-dependent manner based on data characteristics and research objectives (Tasseron et al., 2024). For each simulation output, a binary hotspot mask was generated by applying the threshold to the particle density field. Simulated hotspot maps were then produced for different aggregation modes (e.g., monthly cumulative and mean conditions) to distinguish between transient and persistent accumulation patterns. The spatial extent of simulated hotspots was quantified by counting the number of grid cells exceeding the threshold and converting this to area using the effective cell size (around 0.0087 km^2 per cell), allowing consistent comparison of accumulation zones across scenarios and time periods.

To evaluate the sensitivity of the hotspot definition to the selected threshold, the baseline cumulative particle-density field was additionally analyzed using alternative thresholds of 5 and 20 items m^{-2}, alongside the operational threshold of 10 items m^{-2}. Hotspot cells were classified into three density classes: 5–10, 10–20, and ≥20 items m^{-2}. The number of hotspot cells and their spatial overlap relative to the 10 items m^{-2} threshold were then calculated to assess whether the main model-predicted potential accumulation zones were robust to the threshold choice. Details of the calculation are provided in the SM (Eqs. (S23) and (S24)).

3. Results

3.1. Spatio-temporal drivers of riverine plastic emissions across basins

The monthly riverine plastic emissions estimated by the spatial probabilistic model under three MPW source-intensity sensitivity cases, together with the relative contribution of individual river basins, is presented in Fig. 3. All cases exhibit a consistent seasonal pattern (Fig. 3a), with emissions increasing from winter to spring, reaching a maximum in late spring (April–May), and showing a secondary peak in late autumn (November). Lower emissions are observed during winter and early summer months. For the 2019 baseline-load case, total annual emissions reach 4.23×10^4 kg yr^{-1}, with pronounced peaks in May and November, and lower values during winter and early summer. The high-load source-intensity case shows a similar seasonal pattern but higher overall emissions, corresponding to an increase of approximately 12.6% compared to the baseline. In contrast, the low-load case shows a substantial reduction in emissions, corresponding to a decrease of approximately 82.6% relative to the baseline-load case. Despite these differences in magnitude, all cases exhibit consistent temporal patterns, as expected given that the same environmental forcing is used and only the source intensity is varied. This indicates that seasonality is primarily controlled by environmental forcing, while emission scenarios modulate the overall intensity.

The relative contribution of individual rivers (Fig. 3b) indicates strong spatial heterogeneity in emissions. The Brenta River dominates the system, contributing approximately 37.3% of total emissions, followed by the Sile (12.2%) and Dese (9.8%). Other rivers, such as

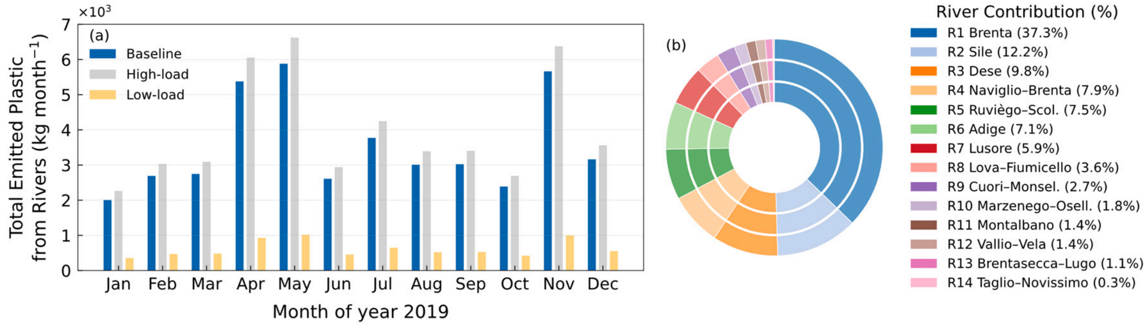

Fig. 3. Riverine plastic emissions under different MPW scenarios. (a) Monthly total plastic emissions from rivers for the three scenarios: Baseline, High-load source-intensity case, and Low-load source-intensity case. (b) Relative contribution of individual rivers to total emissions.

Naviglio–Brenta, Ruviego–Scolmatore, and Adige, contribute moderate shares, while the remaining basins have comparatively minor contributions. Overall, the top six rivers account for more than 80% of total emissions. These results indicate that plastic emissions are unevenly distributed across the study area and are controlled by localized factors such as population density, land use, and hydrological characteristics. This concentration of emissions within a limited number of rivers is consistent with global assessments showing that a small fraction of rivers contributes disproportionately to plastic inputs to the ocean (Meijer et al., 2021; Strokal et al., 2023). The amount of emissions in a limited number of river basins suggests that targeted mitigation strategies focusing on key sources could significantly reduce plastic inputs to the lagoon system.

To further investigate the drivers of plastic emissions, Fig. 4 shows the monthly variability of emissions for the four dominant rivers together with key environmental forcing variables, including precipitation, wind speed, and river water discharge. As shown in Fig. 4a–d, all rivers exhibit a consistent seasonal pattern, with emissions increasing sharply during spring (April–May) and showing a secondary peak in late autumn (November). The comparison with environmental variables (Fig. 4e–h) indicates that these emission peaks coincide with periods of increased precipitation and river discharge. For example, in the Brenta basin, precipitation rises from around 14 mm in January to over 220 mm in May, while discharge rises from around 57 $m^3\ s^{-1}$ to over 265 $m^3\ s^{-1}$, coinciding with a marked increase in plastic emissions. An even stronger peak is observed in November, where precipitation reaches around 308 mm and discharge exceeds 350 $m^3\ s^{-1}$, corresponding to one of the highest emission values of the year. Similar relationships between discharge peaks and plastic transport have been observed in field studies, where riverine plastic flux increases significantly during high-

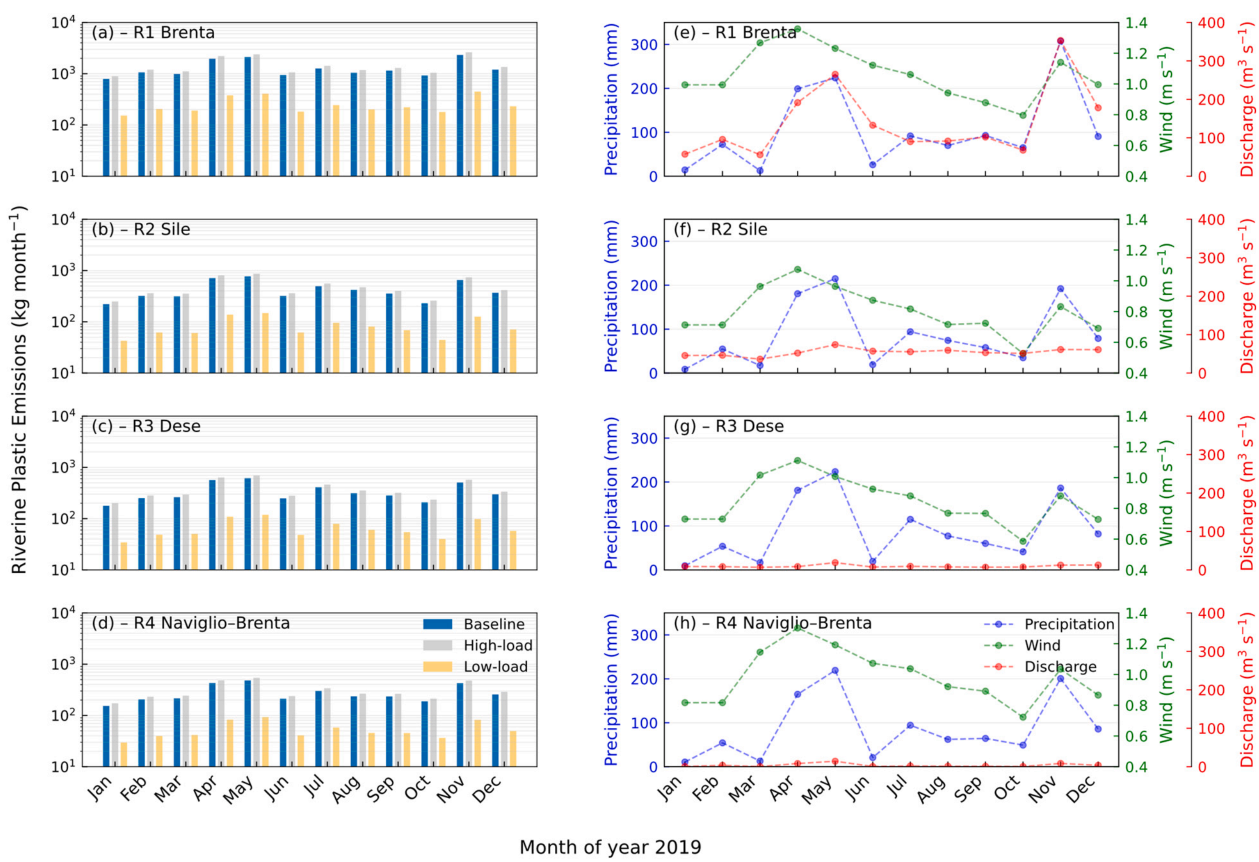

Fig. 4. Monthly plastic emissions and environmental drivers for the main contributing rivers. Left panels (a–c) show monthly plastic emissions for the four dominant rivers, Brenta, Sile, Dese, and Naviglio–Brenta, under the three scenarios: Baseline, High-load, and Low-load. Right panels (e–h) show the corresponding monthly precipitation, wind speed, and river discharge.

flow conditions and flood events (van Emmerik et al., 2022, 2023). Experimental evidence further indicates that rainfall-driven runoff is a key mechanism for mobilizing plastics, while wind primarily enhances transport when combined with hydrological processes (Mellink et al., 2024).

A similar relationship is observed for the other rivers. In the Sile basin, precipitation peaks at around 215 mm in May, accompanied by increased discharge (around 74 m^3 s^{-1}) and elevated emissions. The Dese and Naviglio–Brenta rivers show comparable patterns, with emission peaks consistently aligned with periods of high rainfall and discharge. While wind speed exhibits a seasonal increase, particularly in March, April, May, and November, its influence on plastic emissions appears to modulate the effects of other primary drivers rather than act independently. For instance, despite relatively high wind speeds in March, plastic emissions remain moderate because precipitation and river discharge are still low. In contrast, during April, May, and November, when wind, precipitation, and discharge simultaneously reach high values, plastic emissions show their strongest peaks. This indicates that wind alone is not sufficient to drive significant plastic mobilization, but it can enhance transport processes when combined with strong hydrological forcing. Overall, the highest emission periods occur when all three drivers—precipitation, discharge, and wind—are elevated. This finding is consistent with the probabilistic formulation of the SPM, where mobilization and transport probabilities increase with rainfall and river discharge. The limited role of wind alone is in line with recent findings that hydrometeorological variables often show weak independent correlations with plastic transport, but become significant when acting jointly (Mellink et al., 2024; Pinto et al., 2024).

The spatial variability of plastic emissions across river basins (Table 1 and Table S6) reflects the combined influence of MPW and transport efficiency, as represented by the probabilistic components of the model (Eqs. (S1)–(S5)). The results confirm a strong heterogeneity in emissions, with values spanning over two orders of magnitude, from 107 kg yr^{-1} (Taglio–Novissimo) to 15,776 kg yr^{-1} (Brenta). Larger and more populated basins generate higher MPW and therefore tend to produce higher emissions, which is consistent with studies identifying MPW as a primary predictor of plastic pollution levels in river systems (Pinto et al., 2024). This is evident for the Brenta River, which, with the largest basin area (4607 km^2) and population (around 1.54 million), produces the highest MPW (1.73×10^5 kg yr^{-1}) and consequently the largest emission, despite having a moderate emission probability ($P_{(E)} =$ 0.76%).

However, this relationship is not universal. A notable example is the comparison between the Adige and Dese rivers. Although the Adige has a larger population and higher MPW values, the Dese produces higher emissions than the Adige as shown in Fig. S9. This difference is explained by the transport probabilities. The Adige has a much longer transport distance to the sea ($D_R = 108$ km) compared to the Dese ($D_R =$ 21 km), which substantially reduces its probability of transport to the sea ($P_{(O)}$ = 39% vs 81% for Dese), despite its much higher discharge (226 m^3 s^{-1} vs 9.6 m^3 s^{-1}). A similar contrast can be observed between rivers with high transport efficiency but relatively low MPW. For instance, the Ruviego–Scolmatore exhibits the highest emission probability ($P_{(E)}$ = 1.81%) due to a combination of high $P_{(R)}$ and $P_{(O)}$ (short distances to river and sea, and efficient routing). As a result, it produces emissions (3189 kg yr^{-1}) comparable to larger basins, despite a much lower MPW.

The mobilization probability $P_{(M)}$ varies only slightly across basins (2.7–3.9%), reflecting relatively uniform climatic forcing across the region. In contrast, the transport-related probabilities show much larger variability. The probability of transport to rivers $P_{(R)}$ is primarily controlled by terrain characteristics and distance to the river network, increasing in areas with favorable slopes and shorter pathways. The probability of transport to the sea $P_{(O)}$ is strongly influenced by hydrological variables, decreasing exponentially with increasing distance to the sea while being enhanced by higher discharge and stream order (Table 1; Table S6). As a result, basins with similar MPW can produce markedly different emissions due to differences in transport efficiency, explaining why emission hotspots are not necessarily associated with the largest or most populated rivers.

When emissions are normalized by basin area (Table S6), additional patterns emerge. Smaller basins such as Ruviego–Scolmatore show very high values of MPW/A (>160 kg km^{-2} yr^{-1}) and M_E/A (>35 kg km^{-2} yr^{-1}), indicating intense localized pressure and efficient transport. In contrast, large basins such as the Adige exhibit much lower values (M_E/A = 2.3 kg km^{-2} yr^{-1}), reflecting dilution effects and reduced transport efficiency.

These findings highlight two distinct types of priority areas. First, high-MPW basins such as the Brenta, where large population and MPW drive the highest absolute emissions, should be prioritized for interventions aimed at reducing plastic production and improving waste management. Second, high-efficiency basins such as Ruviego–Scolmatore and Dese, where a relatively large fraction of generated plastic is transported to the lagoon, should be prioritized for targeted measures such as interception systems, riverbank retention, or local barriers.

Table 1

Characteristics of river basins and estimated plastic emissions to the river–sea system. The table reports basin area, population, and annual MPW, together with the average distances from land to the river network (D_L) and along the river network to the sea outlet (D_R). The probability of plastic emission to the river–sea system ($P_{(E)}$) represents the combined effect of mobilization, transport to rivers, and riverine transport. The ratio M_E/MPW indicates the effective transport efficiency from land to the lagoon–sea system. The sum row reports only additive variables; non-additive variables such as distance metrics, average probability, and ME/MPW are not summed.

ID	Rivers name	Basin area (km^2)	Annual mean population	MPW (kg $year^{-1}$)	D_L (km)	D_R (km)	Average P(E) (%)	M_E (kg $year^{-1}$)	M_E/ MPW
R1	Brenta	4606.87	1,539,927	173,142.18	1.05	73.34	0.76	15,775.84	9.11
R2	Sile	743.52	374,898	42,146.09	1.26	32.37	1.03	5182.39	12.30
R3	Dese	297.23	208,607	23,453.76	0.71	21.17	1.47	4144.83	17.67
R4	Naviglio–Brenta	309.70	181,324	20,369.47	0.94	27.24	1.37	3344.48	16.42
R5	Ruviego–Scolmatore	91.04	130,503	14,662.26	0.76	11.34	1.81	3188.57	21.75
R6	Adige	1314.09	386,435	43,452.76	0.83	107.86	0.47	2990.21	6.88
R7	Lusore	161.17	124,594	14,004.26	1.17	13.65	1.48	2483.16	17.73
R8	Lova–Fiumicello–Fiumazzo	146.98	116,380	13,075.36	2.68	12.82	0.96	1508.59	11.54
R9	Cuori–Monselesana–Trezze	482.95	99,382	11,175.89	2.13	22.08	0.86	1155.78	10.34
R10	Marzenego–Osellino Channel	52.17	32,658	3669.15	0.61	22.68	1.74	765.47	20.86
R11	Montalbano	88.28	29,403	3303.75	1.41	15.58	1.55	612.84	18.55
R12	Vallio–Vela–Silone	110.06	31,209	3512.19	0.94	12.98	1.42	596.69	16.99
R13	Brentasecca–Lugo Channel	43.77	20,425	2296.77	0.88	6.04	1.72	473.78	20.63
R14	Taglio–Novissimo	23.98	4830	542.89	1.25	5.87	1.65	107.14	19.74
Sum of included rivers		8471.81	3,280,575	368,806.78				42,329.77	

3.2. Consistency and sensitivity of riverine emission estimates

Fig. S10 in the SM compares the annual riverine plastic emissions estimated in this study with those reported by Meijer et al. (2021) and Mai et al. (2023). This comparison is intended as a cross-model consistency check rather than as a validation exercise, since both reference datasets are derived from modeling frameworks and do not represent independent observational measurements. Overall, the results from this study and Meijer et al. (2021) are comparable in both magnitude and ranking of the main contributing rivers, particularly for the Dese River (4144.83 in this study vs 4100 kg yr^{-1}). The comparison with Mai et al. (2023) is available only for Brenta and Adige and shows substantially higher values, especially for Adige. This discrepancy is expected because Mai et al. (2023) estimated total riverine plastic outflows using a global River-to-Ocean modeling framework based on country- and basin-scale socioeconomic indicators, including plastic waste generation, population, Human Development Index, and exported plastic fractions, with estimates referring to 2016. The present study represents conditions in 2019, whereas the estimates of Meijer et al. (2021) represent conditions in 2015, which may reflect differences in waste generation and hydrological conditions. In addition, the present model is implemented at a much higher spatial (10 m) and temporal (monthly) resolution and uses region-specific datasets, allowing for a more detailed representation of transport processes at the basin scale. The discrepancy observed for the Adige River is likely related to the spatial domain considered in this study, which focuses on the lower portion of the basin within the Veneto region, rather than the entire catchment. This results in a reduced MPW input and consequently lowers estimated emissions.

The OAT analysis showed broadly similar sensitivity patterns for the Brenta and Dese rivers (Fig. 5). Annual emission estimates were particularly sensitive to the mobilization parameters α and β. Increasing the wind coefficient β produced the largest positive response, increasing annual M_E by approximately a factor of 6.4 in Brenta and 6.1 in Dese relative to baseline. Increasing the precipitation coefficient α also strongly increased annual emissions, by approximately a factor of 4.6 in Brenta and 4.9 in Dese. Conversely, reducing β or α decreased annual emissions by approximately 36–54%, depending on the river. The lower-threshold river transport parameters μ and ι produced the strongest negative responses when reduced. Decreasing μ or ι by one order of magnitude reduced annual M_E by about 91% in Brenta and 83% in Dese, indicating that the model is highly sensitive to the assumed minimum probability of downstream riverine transport. However, increasing ι had little effect because the parameter was capped at 1, and the reference value was already close to unity. The land-use coefficient ν had an intermediate effect, reducing ν decreased emissions by about 54% in Brenta and 50% in Dese, while increasing it enhanced emissions by about 99% in Brenta and 46% in Dese. In contrast, the stream-order coefficient θ, discharge coefficient κ, and slope threshold τ produced comparatively small changes in annual emissions.

The regional sensitivity analysis showed that parameter changes affected both total annual emissions and, in some cases, the relative ranking of contributing rivers (Fig. 6). Reducing either of lower river-transport thresholds, ι or μ, produced the strongest response, decreasing total annual emissions by 98.8% and substantially reorganizing the river ranking. Increasing μ produced the largest positive response (+63.5%) and caused moderate ranking changes, whereas the upper configuration of ι increased total emissions by only 3.1%. Variations in the wind, land-use, and precipitation coefficients resulted in more moderate total-emission changes of approximately ±30%, ±25%, and ±20%, respectively, with generally limited effects on river ranking.

The Spearman correlation analysis showed similar patterns for the Brenta and Dese basins (Fig. S11). Monthly emissions were most strongly associated with precipitation ($\rho = 0.93$ and 0.94), followed by discharge ($\rho = 0.84$ and 0.83), while wind showed weaker associations ($\rho = 0.51$ and 0.57, respectively).

The daily-resolution sensitivity analysis showed that sub-monthly discharge variability can redistribute riverine emissions within a single month. In November 2019, normalized discharge in the Brenta River ranged from well below the monthly mean to more than 2.5 times the monthly mean, with the strongest peak occurring on day 16. The Dese River showed less pronounced but still substantial discharge variability, with a maximum daily discharge approximately 1.8 times the monthly mean. These discharge anomalies produced corresponding changes in the daily allocation of M_E relative to a uniform daily release. For Brenta,

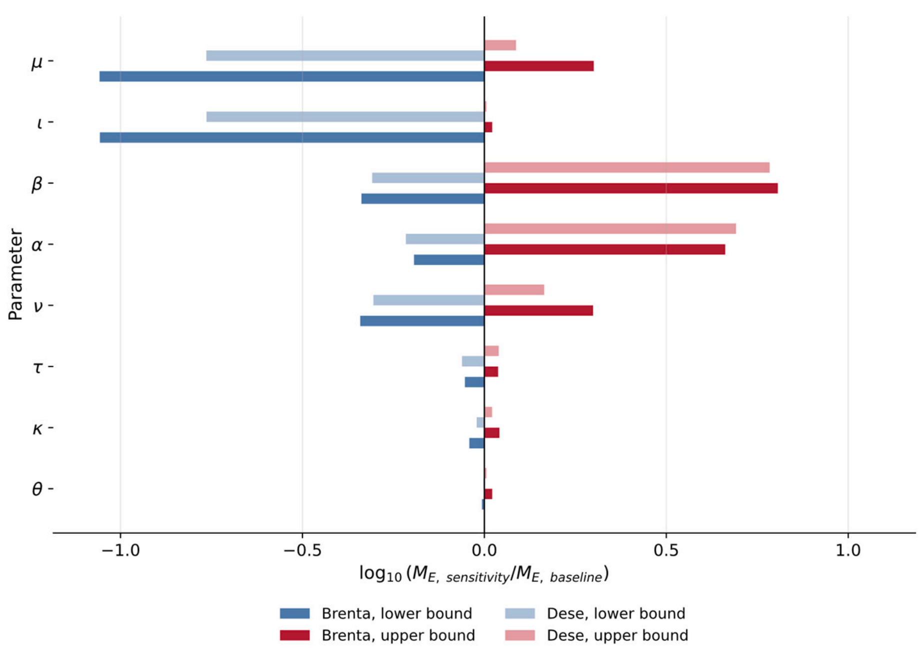

Fig. 5. One-at-a-time sensitivity of annual macroplastic emission estimates for the Brenta and Dese rivers. Bars show the response of annual macroplastic emission, M_E, to individual parameter perturbations relative to the baseline configuration, expressed as $\log_{10}(M_{E,\text{sensitivity}}/M_{E,\text{baseline}})$. Negative values indicate a reduction in estimated emissions relative to baseline, while positive values indicate an increase. Lower-bound simulations correspond to parameter values divided by 10, whereas upper-bound simulations correspond to parameter values multiplied by 10, with probability-threshold parameters capped at 1.

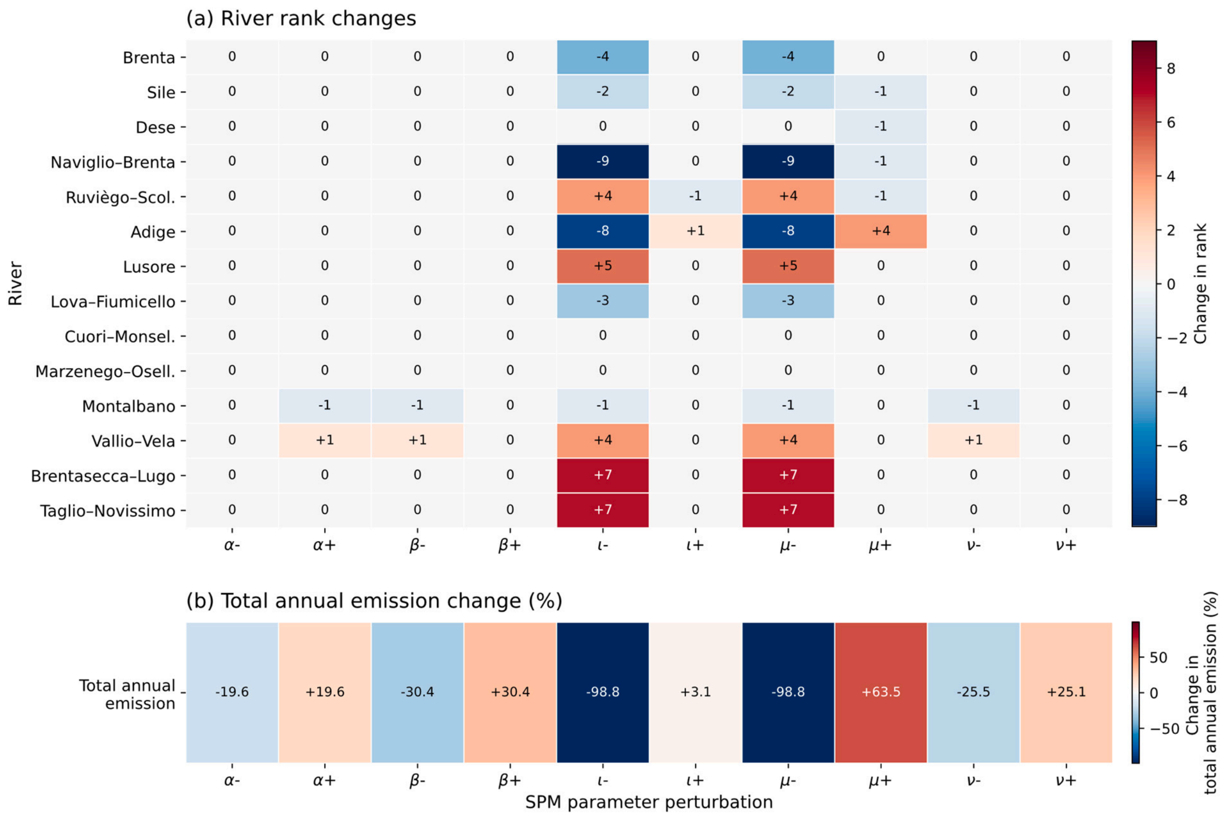

Fig. 6. Regional sensitivity of annual riverine macroplastic emissions and river rankings to variations in the most influential parameters of the spatial probabilistic model. (a) Changes in the annual emission ranking of individual rivers relative to the baseline configuration. Positive values indicate movement to a higher rank, negative values indicate movement to a lower rank, and zero indicates no change. (b) Percentage change in total annual riverine macroplastic emissions relative to the baseline configuration. The symbols α, β, ι, μ, and ν denote the precipitation coefficient, wind coefficient, stream-order lower threshold, discharge lower threshold, and land-use coefficient, respectively. The signs − and + indicate parameter values reduced by 50% and increased by 50% relative to the baseline, respectively. For probability parameters bounded between 0 and 1, the upper parameter value was capped at 1.

daily deviations ranged from approximately −30% during low-flow days to +79% during the main discharge peak, while Dese showed deviations from about −14% to +56%. Despite this redistribution, the total monthly M_E changed only marginally, with cumulative daily values differing by less than approximately 5% from the baseline monthly estimate for both rivers. This indicates that monthly emission estimates may smooth substantial event-scale variability in the timing of riverine plastic delivery, even when the total monthly emission is held constant or only slightly modified in the sensitivity framework. The results of this sensitivity analysis are provided in the Supplementary Material (Figs. S12 and S13).

3.3. Baseline particle accumulation and simulated hotspot patterns

The spatial distribution of particle density and model-predicted potential accumulation zones, hereafter also referred to as simulated potential accumulation hotspots, derived from the Lagrangian simulations for the baseline scenario is reported in Fig. 7. The cumulative particle density map (Fig. 7a) reveals strong spatial heterogeneity, with the highest concentrations occurring within the lagoon, particularly along the main channels and near river inflow areas, while lower densities are observed on the adjacent Adriatic shelf. Annual cumulative particle density was calculated by aggregating the monthly gridded density maps (Table S7). Across non-zero grid cells, particle density ranged from 1.14 to 1474.97 items m^{-2} for the full column, with a mean value of 42.51 items m^{-2}. The bottom layer showed a higher mean density (70.20 items m^{-2}) than the water column (20.60 items m^{-2}), supporting the stronger contribution of bottom-associated accumulation to the overall density pattern. A clear offshore transport pathway is visible outside the lagoon, forming elongated plume-like structures that follow the dominant circulation patterns. The hotspot analysis (Fig. 7b–d) further highlights the preferential accumulation of particles within the lagoon system. Based on the monthly cumulative simulated potential accumulation hotspot map (Fig. 7b), a total of 3234 hotspot cells are identified, of which around 85% are located within the lagoon and only around 15% on the shelf. This corresponds to a total hotspot area of 28.1 km^2, with 24.0 km^2 inside the lagoon and 4.1 km^2 offshore. The strong confinement of model-predicted potential accumulation zones within the lagoon reflects the limited water exchange and the presence of trapping zones, which are characteristic of semi-enclosed basins such as the Venice Lagoon (Cucco and Umgiesser, 2015).

The distinction between bottom layer and water column simulated potential accumulation hotspots provides further insight into vertical transport processes. A substantial fraction of these simulated hotspots is associated with the bottom layer (1993 cells, around 62% of total cumulative simulated hotspots), suggesting that particle settling and near-bed transport play a key role in accumulation. It should be noted that resuspension processes are not included in the model, and therefore bottom retention may be overestimated. In contrast, water column simulated hotspots (1241 cells) are more spatially dispersed and represent more transient accumulation patterns. This vertical differentiation indicates that once particles sink, they are more likely to remain trapped within the lagoon due to reduced velocities near the bed. Similar retention mechanisms have been observed in tidal river and estuarine systems, where plastics undergo repeated cycles of transport, trapping, and remobilization, leading to long residence times and localized accumulation (Lotcheris et al., 2024). Preferential accumulation on the lagoon floor is also consistent with observations of microplastic

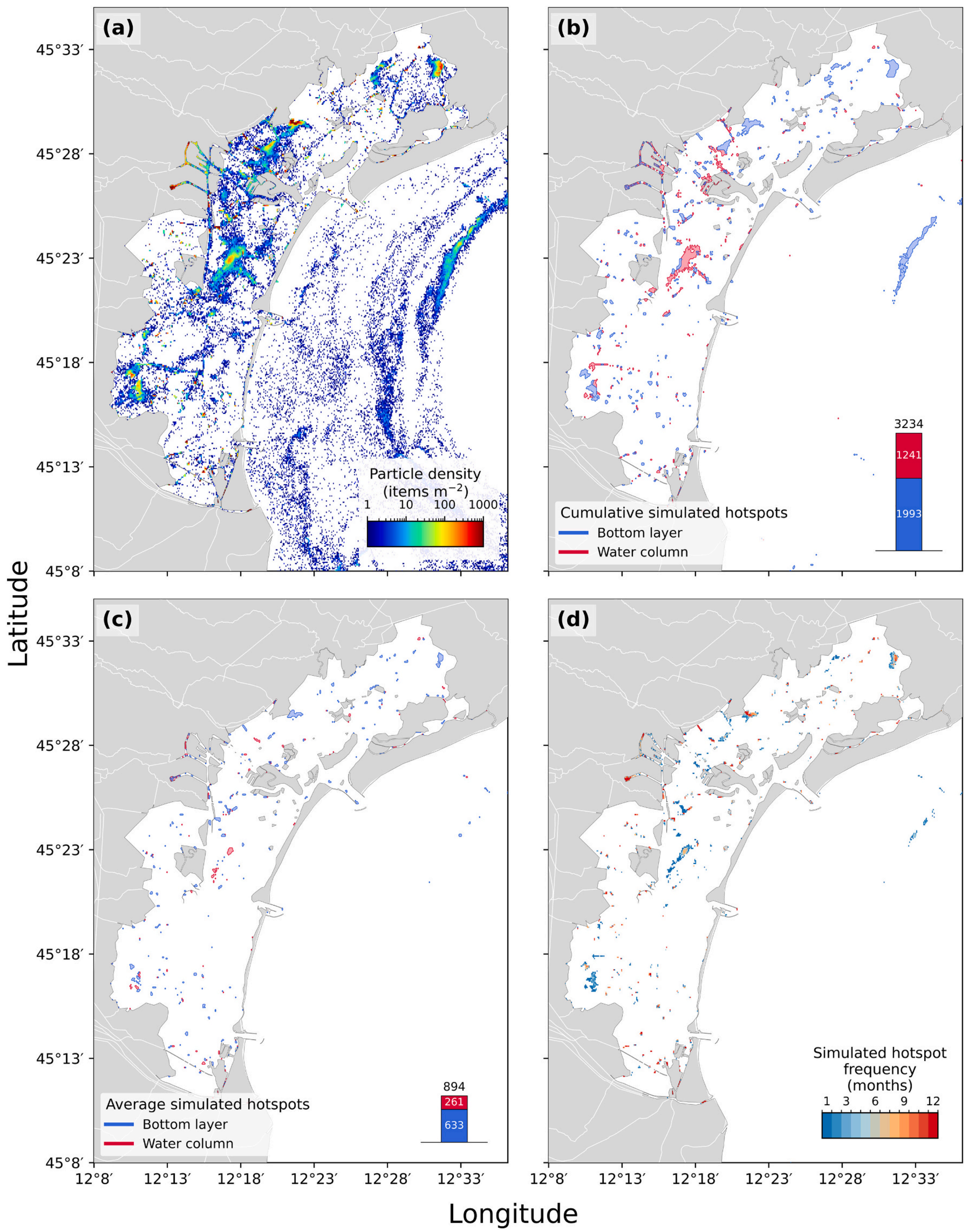

Fig. 7. Spatial distribution of particle density and model-predicted potential accumulation zones under Baseline scenario. (a) Monthly cumulative particle density (items m^{-2}) for the full water column. (b) Monthly cumulative simulated hotspots, distinguishing bottom layer and water column, identified using a threshold of ≥10 items m^{-2}. (c) Monthly averaged simulated hotspots. (d) Potential accumulation-zone frequency (number of months).

enrichment in fine sediments within sheltered areas of the Venice Lagoon (Vianello et al., 2013).

The map of monthly average simulated hotspot distribution (Fig. 7c) shows a much more restricted spatial extent compared to cumulative simulated hotspots, with only 894 cells (around 7.8 km^2) exceeding the threshold on average. Importantly, more than 95% of these average simulated hotspots are located within the lagoon, confirming that persistent model-predicted potential accumulation zones are strongly confined to the lagoon interior. In contrast, hotspot presence on the shelf is limited and highly intermittent. The simulated hotspot frequency map (Fig. 7d) further supports this interpretation, showing that the most persistent simulated potential accumulation hotspots (up to 12 months of occurrence) are concentrated in specific lagoon areas. Offshore areas, in contrast, exhibit low-frequency simulated hotspots, indicating that particle presence on the shelf is more transient and controlled by episodic transport events.

The monthly evolution under the baseline scenario (Fig. 8a and Figs. S14 and S15) reveals a marked seasonal variability that closely

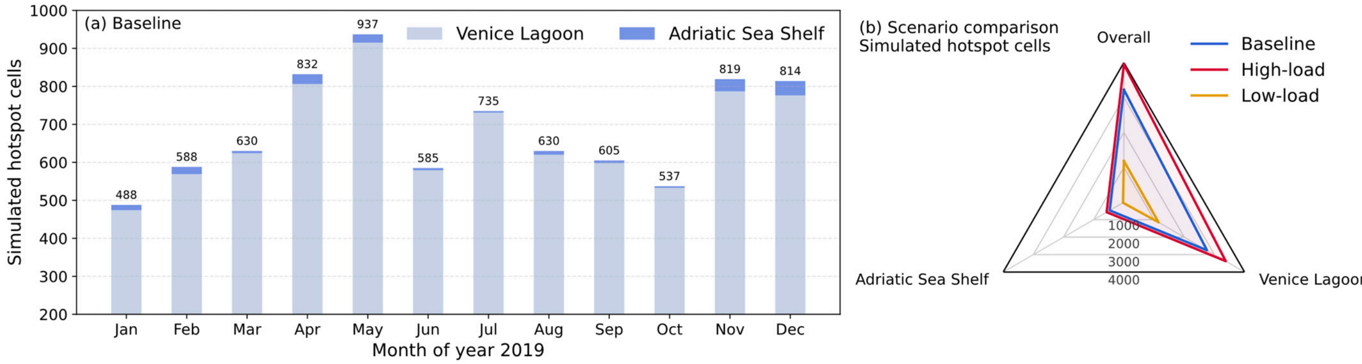

Fig. 8. Summary of model-predicted potential accumulation-zone statistics. (a) Monthly simulated hotspot extent under the baseline scenario, showing contributions from the Venice Lagoon and Adriatic Sea shelf. (b) Scenario comparison (Baseline, High-load, Low-load) for cumulative simulated hotspot extent, including overall, lagoon, and shelf contributions. All extents are based on the ≥10 items m^{-2} threshold.

mirrors the temporal variability of riverine emissions predicted by the SPM. Monthly simulated hotspot extent increases from 488 cells in January to 937 cells in May, then decreases during summer, before rising again in November (819 cells) and December (814 cells). This seasonal pattern is highly consistent with the monthly plastic emissions estimated from the probabilistic model, which also peak in April–May and show a secondary increase in November. The correspondence between emission peaks and the expansion of simulated potential

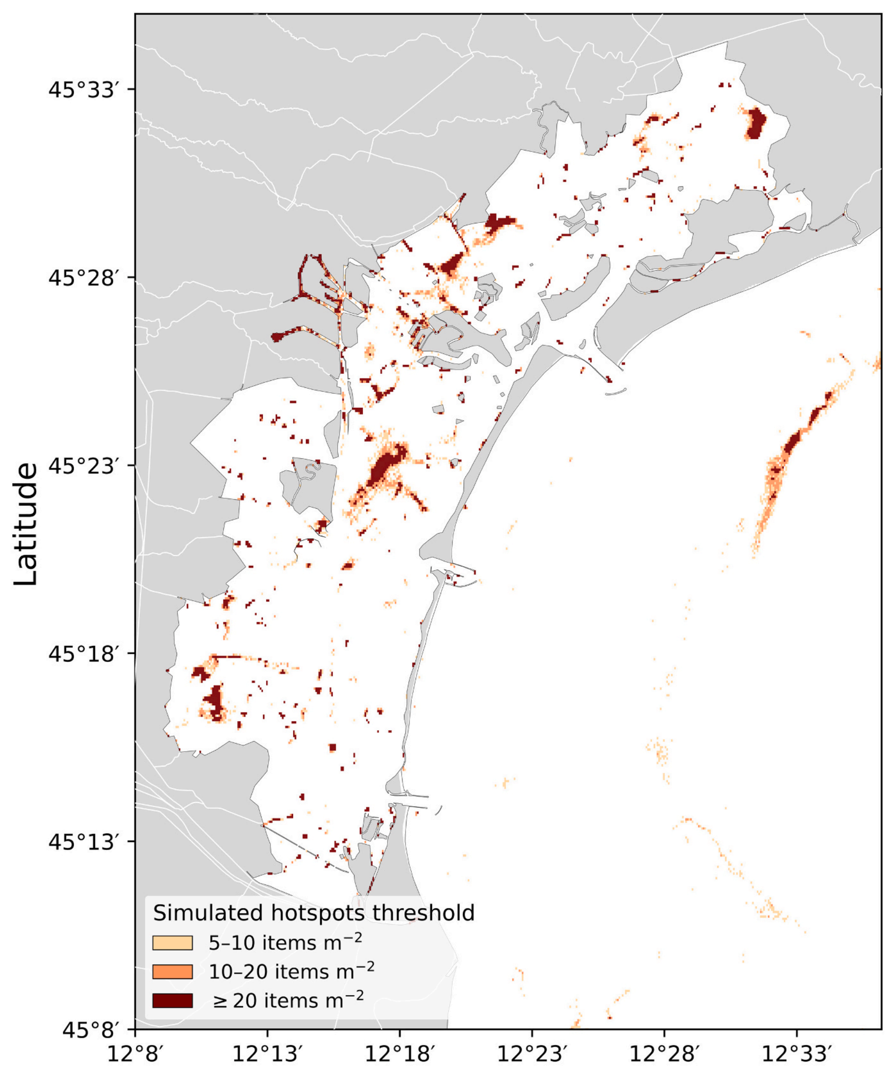

Fig. 9. Threshold sensitivity of model-predicted potential accumulation zones under the baseline scenario. Hotspot classes are shown for the annual cumulative particle-density field using thresholds of 5, 10, and 20 items m^{-2}.

accumulation hotspots indicates that periods of high mobilization and transport from river basins translate directly into larger model-predicted potential accumulation zones in the lagoon. In particular, May, which showed the highest riverine emissions in the SPM, also exhibits the largest hotspot extent (937 cells; 7.97 km^2 in the lagoon). Likewise, the late-autumn increase in SPM emissions is reflected in the November–December expansion of simulated potential accumulation hotspots. This temporal consistency supports the interpretation that the Lagrangian accumulation patterns are dynamically linked to the source variability estimated by the land-based emission model.

The threshold-sensitivity analysis showed that hotspot extent decreased with increasing threshold, as expected. Under the baseline cumulative simulation, the number of hotspot cells decreased from 4872 cells at ≥5 items m^{-2} to 3234 cells at ≥10 items m^{-2} and 1943 cells at ≥20 items m^{-2}. This corresponds to a 50.6% increase when using the lower 5 items m^{-2} threshold relative to the operational 10 items m^{-2} threshold, and a 39.9% decrease when using the higher 20 items m^{-2} threshold. However, the main hotspot locations remained spatially consistent, with the ≥20 items m^{-2} threshold identifying the core of the same accumulation zones detected using the operational 10 items m^{-2} threshold. This indicates that hotspot extent is threshold-dependent, while the location of the main model-predicted potential accumulation zones is robust to the tested thresholds (Fig. 9; Table 2).

The settling-velocity sensitivity analysis showed that model-predicted accumulation patterns were strongly affected by the assumed particle settling behavior (Fig. S16; Tables 3 and S8). The fraction of the cumulative particle-density metric associated with the bottom layer increased from 35.69% for the slow-settling case (1×10^{-5} m s^{-1}), to 54.45% in the baseline case (1×10^{-4} m s^{-1}), and to 70.82% for the fast-settling case (1×10^{-3} m s^{-1}) (Table 3). In contrast, the slow-settling case retained a larger proportion of particles in the water column and produced the largest number of water-column hotspot cells. The spatial distribution of hotspots also changed substantially across settling velocities, with low Jaccard overlap values relative to the baseline case, ranging from 0.083 to 0.125 (Table S8). The fast-settling (1×10^{-3} m s-1) case produced fewer but denser and more spatially localized hotspots, as indicated by the reduced number of full-column hotspot cells and the higher mean and median hotspot densities (Table 3; Fig. S16). These results indicate that both vertical partitioning and hotspot location are sensitive to the prescribed settling velocity.

3.4. Source-intensity sensitivity of accumulation patterns and particle fate

The comparison of hotspot distributions across the three source-intensity sensitivity cases (Fig. 10) shows that, as expected given identical transport dynamics, the locations of model-predicted potential accumulation zones remain largely stable, while their extent and intensity vary substantially with source magnitude. In Fig. 10a, the strongest overlap between baseline and high-load simulated hotspots is observed in the central and northern lagoon. The low-load source-intensity case preserves the same core simulated hotspot pattern but with much smaller extent. This indicates that the location of model-predicted potential accumulation zones is primarily controlled by the hydrodynamic structure of the lagoon, whereas their magnitude and spatial expansion are controlled by the riverine plastic input. Fig. 10b confirms this behavior, as the areas identified as simulated potential accumulation hotspots in all three source-intensity cases are concentrated in a limited number of recurrent accumulation zones, while case-specific hotspots are mainly located along the margins of these core areas. In other words, increasing emissions under the high-load case expands and intensifies pre-existing model-predicted potential accumulation zones rather than creating entirely new accumulation patterns.

The quantitative comparison in Fig. 8b supports this interpretation. Under cumulative conditions (full water column), total simulated hotspot extent increases from 28.09 km^2 in the baseline-load case to 34.40 km^2 in the high-load case, corresponding to an increase of about 22%, while it decreases to 10.31 km^2 in the low-load case, equivalent to a reduction of about 63% relative to the baseline-load case. Despite these large differences in total simulated hotspot extent, the partitioning between lagoon and shelf remains similar for the baseline-load and high-load cases, with about 85.5% of hotspot area in the lagoon and about 14.5% on the shelf in both cases. In contrast, the low-load case strongly suppresses offshore accumulation, with 97.4% of cumulative hotspot area inside the lagoon and only 2.6% on the shelf. This shows that reducing riverine inputs is particularly effective in limiting the export and persistence of simulated potential accumulation hotspots outside the lagoon, while the lagoon itself remains the dominant accumulation environment under all source-intensity cases.

Providing an integrated assessment of the particle budget (Fig. 11), a balance between retention within the Venice Lagoon and export toward the Adriatic Sea is evident. A total of approximately 2.38 million particles are introduced over the year in the baseline-load case across the entire model domain (Venice Lagoon and Adriatic shelf), with pronounced peaks in April–May and November. These periods correspond to the highest levels of accumulation observed in previous figures, confirming the strong coupling between emission intensity and in-lagoon particle buildup. A substantial fraction of particles exits the model domain throughout the year, indicating that the system is not closed. About 42.9% of inserted particles leave the domain, while 57.1% remain within the domain. Importantly, among the exited particles, approximately 52.5% originate from inputs that directly enter the Adriatic Sea (e.g., from the Adige River and Adriatic Sea branches of the Brenta and Sile) and subsequently leave the domain. Despite this relatively high exit rate, the lagoon remains the dominant accumulation zone. By the final time step, roughly 94.5% of particles still within the domain are located inside the lagoon, whereas only 5.5% are found on the Adriatic Sea shelf, showing the trapping capacity of the lagoon system. This limited retention on the Adriatic shelf is consistent with the

Table 2
Threshold sensitivity of simulated hotspot extent under the baseline scenario.

Threshold	Hotspot cells	Change relative to 10 items m^{-2}	Jaccard overlap with 10 items m^{-2}
≥5 items m^{-2}	4872	+50.6%	0.645
≥10 items m^{-2}	3234	Reference	1.000
≥20 items m^{-2}	1943	−39.9%	0.618

Table 3
Sensitivity of cumulative particle-density metrics, hotspot counts, and hotspot density to settling velocity. Results are based on cumulative outputs for four representative months: January, May, August, and November.

Metric	Vertical component	Settling velocity		
		10^{-5} m s^{-1}	10^{-4} m s^{-1}	10^{-3} m s^{-1}
Cumulative particle-density (items m^{-2}, grid-cell summed)	Full column	206,859	439,024	482,548
	Bottom	73,831	239,054	341,728
	(fraction, %)	(35.69%)	(54.45%)	(70.82%)
	Water-column	133,028	199,970	140,820
Model-predicted hotspot cells	Full column	1663	1568	443
	Bottom	372	1104	365
	Water-column	1443	493	78
Mean hotspot cells density (items m^{-2})	Full column	62.13	290.65	587.81
	Bottom	176.61	298.87	652.15
	Water-column	61.60	255.98	558.37
Median hotspot cells density (items m^{-2})	Full column	18.35	35.66	88.39
	Bottom	20.64	38.99	88.67
	Water-column	17.21	25.27	78.17

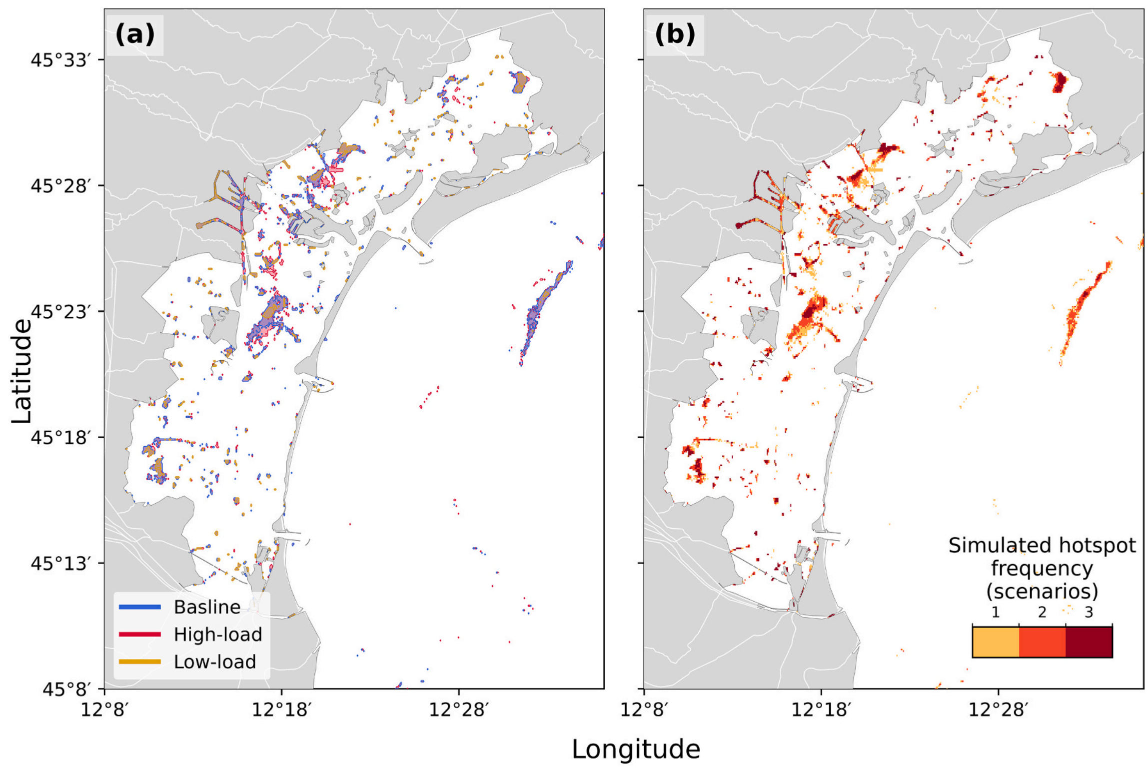

Fig. 10. Comparison of model-predicted potential accumulation-zone distributions across scenarios. (a) Spatial overlap of simulated hotspots for Baseline (blue), High-load (red), and Low-Load (yellow). (b) Simulated hotspot frequency across scenarios, indicating areas consistently identified as potential accumulation zones (1–3 scenarios). All areas are identified using the ≥10 items m^{-2} threshold. (For interpretation of the references to colour in this figure legend, the reader is referred to the web version of this article.)

stronger and more persistent current velocities in the shelf area compared with the lagoon, which enhance particle advection out of the model domain rather than allowing long-term accumulation (Fig. S17).

This behavior is consistent with previous hydrodynamic and Lagrangian studies, which describe coastal lagoons as semi-enclosed systems characterized by strong internal retention and limited exchange with the open sea, controlled by circulation patterns, residence times, and geomorphology (Umgiesser et al., 2014). Comparative studies of systems such as the Mar Menor and the Curonian Lagoon show similarly high internal recirculation and restricted exchange, leading to pronounced retention (Ferrarin et al., 2008; Ghezzo et al., 2015; Pascalis et al., 2012; Pérez-Ruzafa et al., 2005).

The comparison across source-intensity cases (Fig. 11b) shows that changes in source intensity primarily affect the magnitude of the particle budget, while the overall system behavior remains consistent. In the high-load case, total inputs increase to approximately 2.69 million particles, resulting in higher retention within the lagoon (about 1.45 million) and increased export (about 1.15 million). In contrast, the low-load case reduces total inputs to about 0.46 million particles, leading to substantial decreases in both retained (about 0.25 million) and exported particles (about 0.20 million). Despite these differences in magnitude, the relative partitioning between retention and export remains stable across cases, as expected under identical transport dynamics.

4. Discussion

4.1. Integrated river–sea model framework and management implications

This study provides an integrated assessment of macroplastic emissions from inland sources to the coastal ocean through rivers and transitional environments. The results—from the spatial probabilistic model to the Lagrangian transport, accumulation-zone analysis, and particle budget analyses—provide a coherent picture of how plastic propagates through the river–sea system. This framework helps bridge the gap between land-based emission estimates and coastal transport modeling by considering how plastic dynamics are controlled by a combination of source intensity, environmental forcing, and hydrodynamic structure, which together determine when, where, and to what extent accumulation occurs. Temporal variability in emissions strongly influences the magnitude and seasonal expansion of model-predicted potential accumulation zones, whereas the spatial persistence of accumulation zones reflects the dominant role of circulation and morphology. The particle-budget analysis further indicates that particles entering the lagoon–sea system do not follow a single fate pathway. Instead, they are partitioned among retention within the Venice Lagoon, export toward the Adriatic shelf or beyond the model domain, and bottom-associated accumulation. Therefore, the lagoon should be interpreted as an important retention environment, but not as a closed sink.

Climate change, sea-level rise, and the operation of the Mo.S.E. barriers are projected to increase lagoonal residence times (Ferrarin et al., 2022, 2024) and drive persistent alterations of the lagoonal circulation (Rubinetti et al., 2023). However, these processes were not explicitly simulated in the present study, and their potential effects on plastic retention therefore remain an open question and represent a future application of the framework. By linking emissions to transport, our proposed framework can support future investigations of these yet-unresolved dynamics and their role in pollutant accumulation.

Within this context, our findings provide model-based information that may help identify priority areas for management consideration. The strong dependence of particle loads and the extent of model-predicted potential accumulation zones on riverine inputs indicates that reducing emissions at the source—especially in the largest contributing basins—would be expected to reduce overall pollution levels. At the same time, the persistence of recurrent hotspot areas suggests that

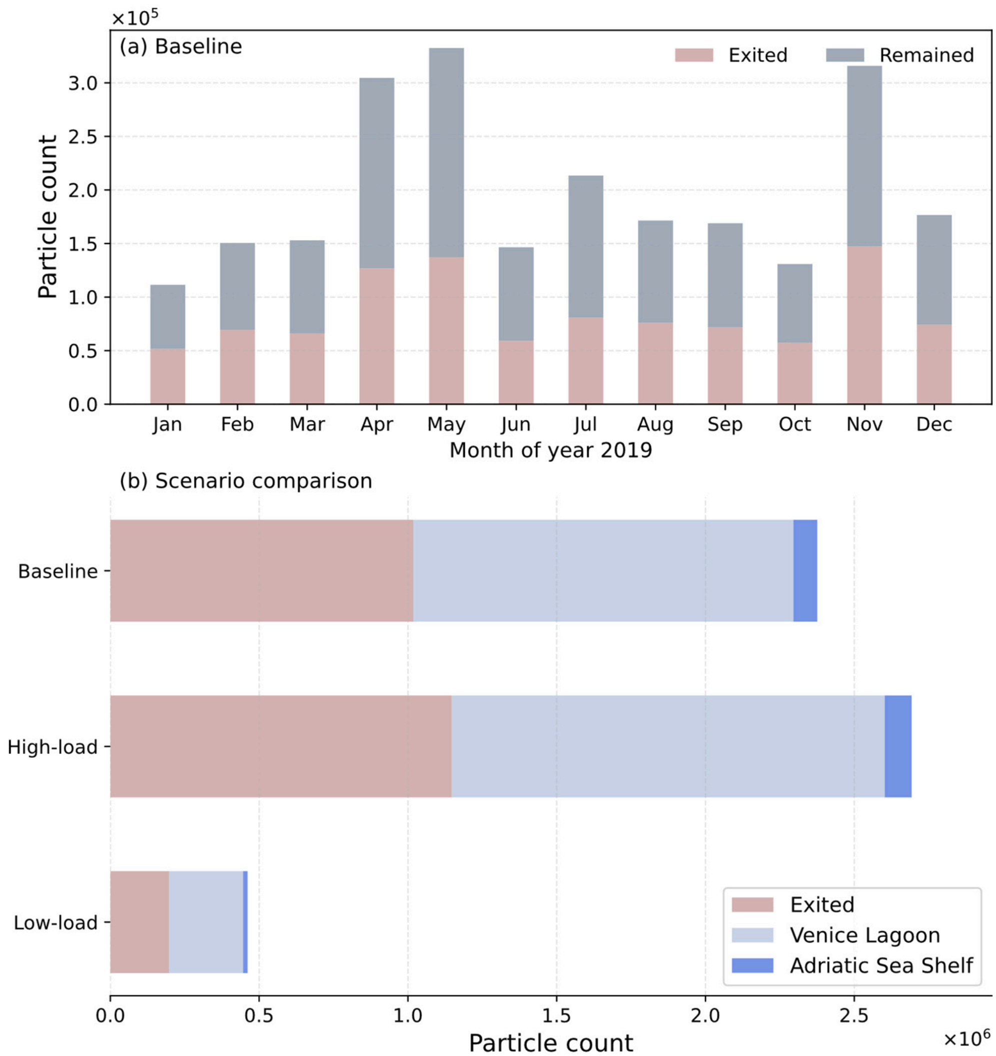

Fig. 11. Particle budget summary. (a) Monthly particle counts under the Baseline scenario, showing contributions from exited particles, Venice Lagoon retention, and Adriatic Sea shelf. (b) Scenario comparison (Baseline, High-load, Low-Load) of total particle counts, highlighting differences in retention and exit among scenarios.

emission reduction alone may not sufficient to eliminate accumulation, as these zones are maintained by intrinsic hydrodynamic retention processes. In transitional systems such as lagoons, circulation patterns, geomorphology, and exchange dynamics create preferential accumulation zones (Cucco and Umgiesser, 2015; Ghezzo et al., 2015). This implies that mitigation planning could benefit from considering both upstream controls and in-system dynamics, including the identification of persistent accumulation zones and the timing of peak transport periods. These findings suggest that plastic-pollution management may benefit from combining source reduction, improved waste management, and transport-based interventions, as emphasized in recent global assessments (Adom, 2026). However, such interventions must be carefully designed, as their effectiveness remains difficult to quantify and interception and removal systems may alter local flow conditions, interfere with sediment transport, or pose risks to aquatic organisms through bycatch or habitat disturbance (Leone et al., 2026).

4.2. Validation limitations and interpretation of model-predicted accumulation zones

A key limitation is that the model-predicted potential accumulation zones could not be directly validated against observations of macroplastic accumulation at comparable spatial and temporal scales. To partially address this limitation, we performed a semi-quantitative comparison between simulated Lagrangian transport pathways and 21 GPS-tracker trajectories collected within the MISP project in the Venice Lagoon. This comparison supported the plausibility of several simulated transport pathways at the lagoon scale, but it should not be interpreted as formal validation because the GPS deployments were carried out in 2025, whereas the hydrodynamic simulation used in this study refers to 2019.

Existing field studies provide useful contextual evidence of plastic contamination in the Venice Lagoon; however, they cannot be used for direct validation of the simulated accumulation zones. The survey of Madricardo et al. (2019) was based on data collected in 2013 and focused on the seafloor of tidal channels and inlets, providing spatially restricted coverage compared with the 2019 lagoon-wide particle transport simulations presented here. In addition, Madricardo et al. (2019) mapped macro-litter on the lagoon seafloor, which may include macroplastic items, whereas the present study simulates macroplastic particle transport and potential accumulation. Therefore, the two datasets differ in temporal coverage, spatial extent, environmental compartment, and represented transport processes, making a direct comparison unsuitable for validation purposes. Similarly, Vianello et al. (2013) investigated small microplastic particles in surface sediments at a limited number of shallow-water sampling sites, which differs from the present model outputs in terms of particle size class, sampling matrix, spatial coverage, and sampling period.

As a result, the simulated patterns should be interpreted as model-predicted potential accumulation zones, rather than as empirically observed hotspots. The comparison with GPS-tracker trajectories provides an observational consistency check of transport pathways, but dedicated observations of macroplastic distribution would be required for direct validation of predicted accumulation zones. Future validation efforts could include targeted litter surveys, shoreline accumulation monitoring, cleanup records, and river monitoring data collected at spatial and temporal scales comparable to the model outputs.

4.3. Uncertainty in riverine emission estimates

Uncertainties in the estimation of riverine inputs propagate through the modeling chain. Although the probabilistic model captures key drivers of plastic mobilization, it does not explicitly account for all processes influencing plastic release. Similar limitations have been highlighted in recent studies, which emphasize the large uncertainty associated with plastic emission estimates (Mellink et al., 2024; Pinto et al., 2024; Roebroek et al., 2022).

The OAT sensitivity analysis provides useful insight into how parameter choices affect the spatial probabilistic emission model, but the results should be interpreted as a local screening exercise rather than as a full uncertainty propagation. For the Brenta and Dese rivers, the annual macroplastic emission estimates were most sensitive to parameters controlling plastic mobilization, particularly the precipitation and wind coefficients, and to parameters defining the lower probability thresholds for riverine transport. The land-use coefficient also influenced the estimated emissions, indicating that assumptions on surface connectivity and land-cover-dependent transport can substantially affect basin-scale plastic inputs.

The subsequent regional sensitivity analysis showed that the ranking of contributing rivers was generally stable under variations in the precipitation, wind, and land-use parameters, whereas changes in the lower river-transport thresholds (ι or μ) substantially altered both total emissions and river ranking. This indicates that source attribution is particularly conditional on assumptions controlling the minimum downstream transport probability and reinforces the need to calibrate these parameters using regional observations.

By contrast, the discharge coefficient κ produced only limited changes in annual M_E under the current reference configuration. This weak response should not be interpreted as evidence that discharge is of minor importance for plastic transport. Rather, it reflects the adopted parameterization, in which κ has a very small reference value and the lower-threshold discharge probability μ is already close to unity. Under these conditions, the discharge-related term has limited leverage on the final river-transport probability, particularly when probabilities approach saturation or are capped at 1. This represents an important structural uncertainty, since flood events and high-discharge periods can strongly influence plastic mobilization and downstream transport in real river systems.

More generally, the sensitivity patterns reported here are conditional on the adopted parameter set. The parameters used in the spatial probabilistic model follow the global framework of Meijer et al. (2021), but they may not be equally representative of regional river–coastal systems. In the absence of local macroplastic emission observations, the present analysis identifies the assumptions that exert the strongest influence around the reference configuration, but it does not provide formal confidence intervals for M_E. Local riverine macroplastic monitoring data would therefore be required to calibrate the emission parameters, reassess model sensitivity under a region-specific configuration, and improve the interpretation of absolute emission magnitudes, source attribution, and downstream accumulation estimates.

The monthly emission estimates should therefore be interpreted as representing seasonal input patterns rather than event-scale plastic delivery. Monthly averaging can smooth short-lived hydrological events and may underestimate short-term pulses in plastic transport. The daily sensitivity analysis showed that observed discharge variability can redistribute emissions within a month, particularly during high-flow periods. However, the total monthly M_E and the cumulative sum of daily M_E in November differed only slightly, again reflecting the limited sensitivity of the current parameterization to discharge variability alone. A full event-scale emission model would require daily spatial predictors for rainfall, wind, and waste mobilization, which were not available in this study. The discharge-related formulation should therefore be reassessed once local observational data become available, as parameters transferred from broader-scale applications may not fully capture river-specific responses in the Venice Lagoon catchments.

4.4. Sensitivity to hotspot threshold and particle properties

The hotspot threshold should be interpreted as an operational criterion rather than an absolute ecological boundary. The sensitivity analysis showed that the estimated hotspot extent changes with the selected threshold, but the main accumulation cores remain spatially stable. This supports the use of the 10 items m^{-2} threshold for identifying model-predicted potential accumulation zones, while highlighting that absolute hotspot area estimates should be interpreted with caution.

Furthermore, the representation of macroplastic particles is simplified. The model assumes uniform properties in terms of size, shape, and buoyancy, while in reality plastic debris exhibits a wide spectrum of characteristics that influence transport behavior. Processes such as fragmentation, biofouling, and degradation can modify buoyancy over time, potentially altering vertical distribution and retention patterns. These processes are not explicitly resolved and may affect the accuracy of long-term transport and accumulation estimates.

The sensitivity analysis confirms that bottom-associated accumulation should be interpreted cautiously since the predicted vertical distribution and hotspot pattern depend strongly on the prescribed settling velocity. In the baseline simulation, more than half of the cumulative particle-density metric was associated with the bottom layer, but this fraction varied substantially across the tested settling velocities. The fast-settling case increased the bottom fraction and concentrated hotspots closer to river mouths, whereas the slow-settling case favored a larger water-column contribution and more extensive water-column hotspots. Moreover, the low hotspot overlap with the baseline case indicates that the spatial pattern of model-predicted potential accumulation zones is not fully robust to this parameter choice. Since resuspension after deposition is not included, bottom-layer accumulation should not be interpreted as permanent benthic storage. Rather, these results represent potential retention zones for simplified macroplastic behavior classes defined by the assumed settling velocity and particle properties.

4.5. Future research and transferability of the framework

Future research should focus on improving both the representation of inputs and the characterization of transport processes. A priority is to quantify the relative contribution of individual rivers to the formation of specific simulated hotspots, as well as to assess the connectivity between source areas and accumulation zones. This could be achieved through targeted Lagrangian experiments and connectivity analyses, allowing a more detailed understanding of source–sink relationships within the lagoon system. Future work should also prioritize dedicated field observations, including riverine plastic monitoring, floating-litter surveys, shoreline accumulation records, and sediment sampling, to verify whether the simulated accumulation patterns correspond to observed macroplastic distributions.

Finally, the extension of the framework to scenario-based simulations—including changes in climate forcing, river discharge, and sea-level conditions—would provide valuable insights into the future evolution of plastic pollution in transitional coastal environments. By integrating land-based emissions with hydrodynamic transport, the approach proposed here offers a flexible methodological framework that can, in principle, be adapted to other lagoon, estuarine, and river–sea systems. However, its transferability should not be interpreted as directly quantitative. Application to other systems, and especially to broader or global scales, would require re-evaluation and recalibration of key assumptions, input datasets, emission parameters, spatial resolution, hydrodynamic forcing, and particle-property settings. Model performance should therefore be reassessed whenever the framework is applied beyond the Venice Lagoon or to larger spatial scales.

5. Conclusions

This study presents an integrated modeling framework linking land-based plastic generation, riverine delivery, and coastal transport within a unified source-to-sink approach. By coupling a spatial probabilistic emission model with a three-dimensional hydrodynamic–Lagrangian transport model (SHYFEM), the framework overcomes the common separation between terrestrial emission estimates and marine transport modeling, explicitly resolving how environmental forcing and human pressures control the magnitude and timing of plastic inputs to coastal systems.

Applied to the Venice Lagoon, selected as a natural laboratory for its strong riverine influence and semi-enclosed hydrodynamics, the framework demonstrates its ability to resolve both the spatiotemporal variability of riverine plastic emissions and their downstream propagation through a complex transitional environment. The results show that plastic inputs are highly uneven among river basins and strongly modulated by seasonal hydrometeorological conditions, with a relatively small number of basins contributing most of the total load.

A key finding is that the magnitude of accumulation responds strongly to changes in riverine inputs, whereas the core location of hotspot areas remains comparatively stable across scenarios. This indicates that source variability controls how much plastic enters and accumulates in the system, while circulation patterns and exchange dynamics largely determine where persistent accumulation occurs. In this respect, the lagoon acts as the primary retention zone, while the adjacent shelf functions mainly as a transport pathway rather than a long-term sink. This distinction is important for management, since it suggests that the spatial distribution of potential accumulation cannot be inferred from source magnitude alone, but must also account for the transport and retention properties of the receiving system.

From a management perspective, these findings highlight that effective mitigation strategies must account for both source dynamics and in-system transport processes. Reducing emissions in the most significant river basins can substantially decrease overall plastic loads entering coastal systems. However, the persistence of hydrodynamically driven accumulation zones indicates that source-control measures alone may not eliminate pollution, as these areas are maintained by intrinsic circulation and retention mechanisms.

By explicitly linking emission areas with transport pathways and accumulation zones, the proposed framework can support the prioritization of monitoring and mitigation efforts in both space and time. It enables the identification of critical source regions, optimal locations for further evaluation of in-system mitigation (e.g., interception or cleanup), and periods of enhanced transport, thereby supporting more targeted and efficient management actions. However, the effectiveness and ecological consequences of specific interventions, such as interception or removal systems, were not directly assessed and would require dedicated field and modeling studies.

The results demonstrate that integrating land-based emissions with coastal transport processes can improve the interpretation of plastic pathways in river-dominated and semi-enclosed coastal systems. The framework offers a flexible basis for future scenario testing and management-oriented applications, but quantitative transfer to other systems requires local calibration, validation, and reassessment of key emission and particle-transport parameters.

CRediT authorship contribution statement

Ali Aalifar: Writing – review & editing, Writing – original draft, Visualization, Validation, Software, Methodology, Investigation, Formal analysis, Data curation, Conceptualization. **William Mc Kiver:** Writing – review & editing, Visualization, Supervision, Software, Methodology, Investigation. **Christian Ferrarin:** Writing – review & editing, Supervision, Software, Resources, Methodology. **Francesca De Pascalis:** Writing – review & editing, Supervision, Software, Resources, Methodology. **Francesco Falcieri:** Writing – review & editing, Supervision, Resources. **Davide Zanchettin:** Writing – review & editing, Supervision, Investigation. **Fantina Madricardo:** Writing – review & editing, Supervision, Resources. **Vanessa Moschino:** Writing – review & editing, Supervision, Resources. **Michol Ghezzo:** Writing – review & editing, Visualization, Supervision, Software, Resources, Methodology, Investigation.

Declaration of competing interest

The authors declare that they have no known competing financial interests or personal relationships that could have appeared to influence the work reported in this paper.

Acknowledgements

This scientific research was partially supported by previous activities in the Research Programme Venezia 2021, coordinated by CORILA (Consortium for coordination of research activities concerning the Venice lagoon system), with the contribution of the Provveditorato for the Public Works of Veneto, Trentino Alto Adige and Friuli Venezia Giulia. The DANUBIUS-RI (The International Centre for Advanced Studies on River-Sea Systems) supported the PhD research focused on land-sea continuum and the H2020 project MAELSTROM (Smart technology for MArinE Litter SusTainable RemOval and Management) contributed to the baseline knowledge of the study. The authors sincerely thank the Editor and the anonymous Reviewers for their constructive comments and suggestions, which helped improve the clarity and scientific robustness of the manuscript.

Appendix A. Supplementary data

Supplementary data to this article can be found online at https://doi.org/10.1016/j.marpolbul.2026.120182.

Data and code availability

The public datasets used to configure the spatial probabilistic emission model and the hydrodynamic–Lagrangian simulations are cited in the manuscript and Supplementary Material, including data sources for population, land use, river networks, basin boundaries, meteorological forcing, river discharge, bathymetry, and open-boundary oceanographic conditions. Model parameter values and equations used in the spatial probabilistic model, sensitivity analyses, hotspot-threshold analysis, and trajectory-comparison metrics are provided in the Supplementary Material.

Processed riverine plastic-emission estimates, parameter tables, scripts used for post-processing and figure generation, and selected gridded outputs supporting the main results can be made available by the corresponding author upon reasonable request. The SHYFEM model is publicly available at https://github.com/shyfemcm.

References

Adom, R.K., 2026. Understanding the socioeconomic determinants of marine plastic pollution: evaluating policy effectiveness and mitigation strategies in the Global South. Mar. Pollut. Bull. 228, 119553. https://doi.org/10.1016/j.marpolbul.2026.119553.

Aghito, M., Calgaro, L., Dagestad, K.-F., Ferrarin, C., Marcomini, A., Breivik, Ø., Hole, L. R., 2023. ChemicalDrift 1.0: an open-source Lagrangian chemical-fate and transport model for organic aquatic pollutants. Geosci. Model Dev. 16, 2477–2494. https://doi.org/10.5194/gmd-16-2477-2023.

Arpaia, L., Ferrarin, C., Bajo, M., Umgiesser, G., 2023. A flexible z-layers approach for the accurate representation of free surface flows in a coastal ocean model (SHYFEM v. 7_5_71). Geosci. Model Dev. 16, 6899–6919. https://doi.org/10.5194/gmd-16-6899-2023.

ARPAV, 2022a. Grafo Idrografia (elemento idrico), ARPAV Geoportal. https://gaia.arpa.veneto.it/layers/idrografia:geonode:v_idrografia_rete. (Accessed 10 December 2025).

ARPAV, 2022b. Bacini idrografici di dettaglio, ARPAV Geoportal. https://gaia.arpa.veneto.it/layers/idrografia:geonode:v_bacini10kmq. (Accessed 10 December 2025).

Autorità di bacino distrettuale delle Alpi Orientali, 2026. MISP – Misure sperimentali nei corsi d'acqua del Distretto Alpi Orientali per la cattura dei rifiuti galleggianti. Available at:, MISP WebGIS repository. https://misp.nauta-rcs.it/lizmap/www/. (Accessed 1 July 2026).

Bajo, M., Ferrarin, C., Umgiesser, G., Bonometto, A., Coraci, E., 2023. Modelling the barotropic sea level in the Mediterranean Sea using data assimilation. Ocean Sci. 19, 559–579. https://doi.org/10.5194/os-19-559-2023.

Blettler, M.C.M., Shumilova, O.O., Gallitelli, L., Sukhodolov, A.N., 2026. Macroplastic in urban waterways: assessing storage in Berlin's Spree River. Environ. Res. 296, 123990. https://doi.org/10.1016/j.envres.2026.123990.

Bondesan, A., 2017. Geomorphological processes and landscape evolution of the Lagoon of Venice. In: Soldati, M., Marchetti, M. (Eds.), Landscapes and Landforms of Italy. Springer International Publishing, Cham, pp. 181–191. https://doi.org/10.1007/978-3-319-26194-2_15.

Bonometto, A., Feola, A., Rampazzo, F., Gion, C., Berto, D., Ponis, E., Brusà, R.B., 2019. Factors controlling sediment and nutrient fluxes in a small microtidal salt marsh within the Venice Lagoon. Sci. Total Environ. 650, 1832–1845. https://doi.org/10.1016/j.scitotenv.2018.09.142.

Borrelle, S.B., Ringma, J., Law, K.L., Monnahan, C.C., Lebreton, L., McGivern, A., Murphy, E., Jambeck, J., Leonard, G.H., Hilleary, M.A., Eriksen, M., Possingham, H. P., De Frond, H., Gerber, L.R., Polidoro, B., Tahir, A., Bernard, M., Mallos, N., Barnes, M., Rochman, C.M., 2020. Predicted growth in plastic waste exceeds efforts to mitigate plastic pollution. Science 369, 1515–1518. https://doi.org/10.1126/science.aba3656.

Canals, M., Pham, C.K., Bergmann, M., Gutow, L., Hanke, G., Van Sebille, E., Angiolillo, M., Buhl-Mortensen, L., Cau, A., Ioakeimidis, C., 2021. The quest for seafloor macrolitter: a critical review of background knowledge, current methods and future prospects. Environ. Res. Lett. 16, 023001. https://doi.org/10.1088/1748-9326/abc6d4.

Carniello, L., Defina, A., D'Alpaos, L., 2009. Morphological evolution of the Venice lagoon: evidence from the past and trend for the future. J. Geophys. Res. 114, 2008JF001157. https://doi.org/10.1029/2008JF001157.

Cecchi, T., Poletto, D., 2025. 'Ghost Boats' in Venice: environmental concerns, green chemical fingerprint, circular and sustainable end-of-life-solutions. Sci. Total Environ. 973, 179126. https://doi.org/10.1016/j.scitotenv.2025.179126.

Cecchi, T., Poletto, D., Berbecaru, A.C., Cârstea, E.M., Râpă, M., 2024. Assessing microplastics and nanoparticles in the surface seawater of Venice Lagoon—part I: methodology of research. Materials (Basel, Switzerland) 17, 1759. https://doi.org/10.3390/ma17081759.

Çevirgen, S., Elwany, H., Pesce, M., Zirino, A., 2020. Managing nutrient pollution in Venice Lagoon (Italy): a practical tool for assessment of water quality. Sustain. Water Resour. Manag. 6, 33. https://doi.org/10.1007/s40899-020-00390-y.

Corbau, C., Skalny, M., Bajda, T., Coustumer, P.L., Marijić, V.F., Lazarou, A., Nardin, W., Coltorti, M., Simeoni, U., 2026. Plastic pollution interception by vegetation: a mechanistic review across diverse habitats. J. Hazard. Mater. 508, 141908. https://doi.org/10.1016/j.jhazmat.2026.141908.

Cottom, J.W., Cook, E., Velis, C.A., 2024. A local-to-global emissions inventory of macroplastic pollution. Nature 633, 101–108. https://doi.org/10.1038/s41586-024-07758-6.

Critchell, K., Lambrechts, J., 2016. Modelling accumulation of marine plastics in the coastal zone; what are the dominant physical processes? Estuar. Coast. Shelf Sci. 171, 111–122. https://doi.org/10.1016/j.ecss.2016.01.036.

Cucco, A., Umgiesser, G., 2015. The Trapping Index: how to integrate the Eulerian and the Lagrangian approach for the computation of the transport time scales of semi-enclosed basins. Mar. Pollut. Bull. 98, 210–220. https://doi.org/10.1016/j.marpolbul.2015.06.048.

Cucco, A., Umgiesser, G., Ferrarin, C., Perilli, A., Canu, D.M., Solidoro, C., 2009. Eulerian and lagrangian transport time scales of a tidal active coastal basin. Ecol. Model. 220 (7), 913–922. https://doi.org/10.1016/j.ecolmodel.2009.01.008.

De Groodt, A., Vieira, L.R., Amorim, F.N., Bio, A., Santos, M., Iglesias, I., 2026. Exposing estuarine regions as microplastic traps: modeling transport pathways and accumulation hotspots in the Minho Estuary (Portugal-Spain). Front. Mar. Sci. 13, 1798554. https://doi.org/10.3389/fmars.2026.1798554.

Escudier, R., Clementi, E., Cipollone, A., Pistoia, J., Drudi, M., Grandi, A., Lyubartsev, V., Lecci, R., Aydogdu, A., Delrosso, D., Omar, M., Masina, S., Coppini, G., Pinardi, N., 2021. A high resolution reanalysis for the Mediterranean Sea. Front. Earth Sci. 9, 702285. https://doi.org/10.3389/feart.2021.702285.

Feola, A., Bonometto, A., Canesso, D., Pedroncini, A., Cacciatore, F., Novello, M., Girolimetto, A., Zorzi, M., Boscolo Brusà, R., 2024. A method to quantify the drainage basin contributions to transitional water bodies: numerical modeling applied to the case study of Venice Lagoon. Environments 11, 234. https://doi.org/10.3390/environments11110234.

Ferrarin, C., Rapaglia, J., Zaggia, L., Umgiesser, G., Zuppi, G.M., 2008. Coincident application of a mass balance of radium and a hydrodynamic model for the seasonal quantification of groundwater flux into the Venice Lagoon, Italy. Mar. Chem. 112, 179–188. https://doi.org/10.1016/j.marchem.2008.08.008.

Ferrarin, C., Ghezzo, M., Umgiesser, G., Tagliapietra, D., Camatti, E., Zaggia, L., Sarretta, A., 2013. Assessing hydrological effects of human interventions on coastal systems: numerical applications to the Venice Lagoon. Hydrol. Earth Syst. Sci. 17, 1733–1748. https://doi.org/10.5194/hess-17-1733-2013.

Ferrarin, C., Maicu, F., Umgiesser, G., 2017. The effect of lagoons on Adriatic Sea tidal dynamics. Ocean Model 119, 57–71. https://doi.org/10.1016/j.ocemod.2017.09.009.

Ferrarin, C., Davolio, S., Bellafiore, D., Ghezzo, M., Maicu, F., Mc Kiver, W., Drofa, O., Umgiesser, G., Bajo, M., De Pascalis, F., 2019. Cross-scale operational oceanography in the Adriatic Sea. J. Oper. Oceanogr. 12, 86–103. https://doi.org/10.1080/1755876X.2019.1576275.

Ferrarin, C., Bajo, M., Benetazzo, A., Cavaleri, L., Chiggiato, J., Davison, S., Davolio, S., Lionello, P., Orlić, M., Umgiesser, G., 2021. Local and large-scale controls of the exceptional Venice floods of November 2019. Prog. Oceanogr. 197, 102628. https://doi.org/10.1016/j.pocean.2021.102628.

Ferrarin, C., Lionello, P., Orlić, M., Raicich, F., Salvadori, G., 2022. Venice as a paradigm of coastal flooding under multiple compound drivers. Sci. Rep. 12, 5754. https://doi.org/10.1038/s41598-022-09652-5.

Ferrarin, C., Bonaldo, D., Bergamasco, A., Ghezzo, M., 2024. Sea level and temperature extremes in a regulated Lagoon of Venice. Front. Clim. 5, 1330388. https://doi.org/10.3389/fclim.2023.1330388.

Ferrarin, C., Bellafiore, D., Paladio Hernandez, A., Dinu, I., Stanica, A., 2025. Modelling river-sea continuum: the case of the Danube Delta. Ocean Sci. 21, 3291–3310. https://doi.org/10.5194/os-21-3291-2025.

Foglini, F., Campiani, E., Cattaneo, A., Correggiari, A., Remia, A., Ridente, D., Trincardi, F., 2012. The Bathymetry of the Adriatic Sea. In: Marine Research at CNR, pp. 445–457.

Gallitelli, L., Scalici, M., 2024. Conceptual model of global plants entrapping plastics. Environ. Rev. 32, 470–484. https://doi.org/10.1139/er-2023-0141.

Gavazzi, G.M., Madricardo, F., Janowski, L., Kruss, A., Blondel, P., Sigovini, M., Foglini, F., 2016. Evaluation of seabed mapping methods for fine-scale classification of extremely shallow benthic habitats – application to the Venice Lagoon, Italy. Estuar. Coast. Shelf Sci. 170, 45–60. https://doi.org/10.1016/j.ecss.2015.12.014.

Ghezzo, M., De Pascalis, F., Umgiesser, G., Zemlys, P., Sigovini, M., Marcos, C., Pérez-Ruzafa, A., 2015. Connectivity in three European coastal lagoons. Estuar. Coasts 38, 1764–1781. https://doi.org/10.1007/s12237-014-9908-0.

Gnann, N., Höreth, K., Schweigert, N., Evers, M., Ternes, T.A., Hamann, L., 2026. The river Rhine transports around 4,000 tonnes of macrolitter towards the North Sea each year. Commun. Sustain. 1, 5. https://doi.org/10.1038/s44458-025-00007-5.

González-Fernández, D., Cózar, A., Hanke, G., Viejo, J., Morales-Caselles, C., Bakiu, R., Barceló, D., Bessa, F., Bruge, A., Cabrera, M., 2021. Floating macrolitter leaked from Europe into the ocean. Nat. Sustain. 4, 474–483. https://doi.org/10.1038/s41893-021-00722-6.

González-Fernández, D., Roebroek, C.T.J., Laufkötter, C., Cózar, A., van Emmerik, T.H. M., 2023. Diverging estimates of river plastic input to the ocean. Nat. Rev. Earth Environ. 4, 424–426. https://doi.org/10.1038/s43017-023-00448-3.

Gündoğdu, S., Köşker, A.R., Akarsu, C., Aydoğan, B., Aydoğan, B., Blettler, M., Büyükdeveci, F., Cvijanović, D., Despina, C., Gallitelli, L., 2026. Micro- and nanoplastic pollution in urban influenced aquatic environments: sources, pathways, and remediation strategies. Mar. Pollut. Bull. 223, 119048. https://doi.org/10.1016/j.marpolbul.2025.119048.

Hardesty, B.D., Harari, J., Isobe, A., Lebreton, L., Maximenko, N., Potemra, J., Van Sebille, E., Vethaak, A.D., Wilcox, C., 2017. Using numerical model simulations to improve the understanding of micro-plastic distribution and pathways in the marine environment. Front. Mar. Sci. 4, 30. https://doi.org/10.3389/fmars.2017.00030.

Haseler, M., Mihut, G., 2026. Two years of daily monitoring of floating macro-litter at the river-sea interface: Aarhus River, Denmark. Mar. Pollut. Bull. 222, 118913. https://doi.org/10.1016/j.marpolbul.2025.118913.

Hurley, R., Braaten, H.F.V., Nizzetto, L., Steindal, E.H., Lin, Y., Clayer, F., van Emmerik, T., Buenaventura, N.T., Eidsvoll, D.P., Økelsrud, A., 2023. Measuring riverine macroplastic: methods, harmonisation, and quality control. Water Res. 235, 119902. https://doi.org/10.1016/j.watres.2023.119902.

ISTAT, 2021. Permanent census of population and housing: the Italian population year 2019. https://www.istat.it/en/infographics/permanent-census-of-population-and-housing-the-italian-population-year-2019/. (Accessed 8 December 2025).

Kaandorp, M.L.A., Dijkstra, H.A., van Sebille, E., 2020. Closing the Mediterranean marine floating plastic mass budget: inverse modeling of sources and sinks. Environ. Sci. Technol. 54, 11980–11989. https://doi.org/10.1021/acs.est.0c01984.

Kaandorp, M.L.A., Lobelle, D., Kehl, C., Dijkstra, H.A., Van Sebille, E., 2023. Global mass of buoyant marine plastics dominated by large long-lived debris. Nat. Geosci. 16, 689–694. https://doi.org/10.1038/s41561-023-01216-0.

Kaimathuruthy, B.J., Jalón-Rojas, I., Sous, D., 2025. Modelling microplastic dynamics in estuaries: a comprehensive review, challenges, and recommendations. Geosci. Model Dev. 18, 7227–7255. https://doi.org/10.5194/gmd-18-7227-2025.

Koelmans, A.A., Kooi, M., Law, K.L., Van Sebille, E., 2017. All is not lost: deriving a top-down mass budget of plastic at sea. Environ. Res. Lett. 12, 114028. https://doi.org/10.1088/1748-9326/aa9500.

Lagomarsino-Oneto, D., De Leo, A., Stocchino, A., Cucco, A., 2024. Unraveling the non-homogeneous dispersion processes in ocean and coastal circulations using a clustering approach. Geophys. Res. Lett. 51, e2023GL107900. https://doi.org/10.1029/2023GL107900.

Lau, W.W.Y., Shiran, Y., Bailey, R.M., Cook, E., Stuchtey, M.R., Koskella, J., Velis, C.A., Godfrey, L., Boucher, J., Murphy, M.B., 2020. Evaluating scenarios toward zero plastic pollution. Science 369, 1455–1461. https://doi.org/10.1126/science.aba9475.

Lebreton, L., Andrady, A., 2019. Future scenarios of global plastic waste generation and disposal. Palgrave Commun. 5, 6. https://doi.org/10.1057/s41599-018-0212-7.

Lebreton, L.C., Van Der Zwet, J., Damsteeg, J.-W., Slat, B., Andrady, A., Reisser, J., 2017. River plastic emissions to the world's oceans. Nat. Commun. 8, 15611. https://doi.org/10.1038/ncomms15611.

Leone, G., Catarino, A.I., Pauwels, I., Bossaer, M., Oco, R.C., Chu, C.-Y., Troch, P., Goethals, P.L.M., Everaert, G., 2026. Plastic clean-up mechanisms: experimental insights on their bycatch. Mar. Pollut. Bull. 226, 119326. https://doi.org/10.1016/j.marpolbul.2026.119326.

Lionello, P., Barriopedro, D., Ferrarin, C., Nicholls, R.J., Orlić, M., Raicich, F., Reale, M., Umgiesser, G., Vousdoukas, M., Zanchettin, D., 2021a. Extreme floods of Venice: characteristics, dynamics, past and future evolution (review article). Nat. Hazards Earth Syst. Sci. 21, 2705–2731. https://doi.org/10.5194/nhess-21-2705-2021.

Lionello, P., Nicholls, R.J., Umgiesser, G., Zanchettin, D., 2021b. Venice flooding and sea level: past evolution, present issues, and future projections (introduction to the special issue). Nat. Hazards Earth Syst. Sci. 21, 2633–2641. https://doi.org/10.5194/nhess-21-2633-2021.

Liro, M., Zielonka, A., Hajdukiewicz, H., Czajka, A., Mikuś, P., Dzida, J., Russell, C., 2025. Rivers as microplastic factories. Environ. Res. Lett. 20, 051005. https://doi.org/10.1088/1748-9326/adca49.

Liubartseva, S., Coppini, G., Lecci, R., Creti, S., 2016. Regional approach to modeling the transport of floating plastic debris in the Adriatic Sea. Mar. Pollut. Bull. 103, 115–127. https://doi.org/10.1016/j.marpolbul.2015.12.031.

Lotcheris, R.A., Schreyers, L.J., Bui, T.K.L., Thi, K.V.L., Nguyen, H.-Q., Vermeulen, B., Van Emmerik, T.H.M., 2024. Plastic does not simply flow into the sea: river transport dynamics affected by tides and floating plants. Environ. Pollut. 345, 123524. https://doi.org/10.1016/j.envpol.2024.123524.

Madricardo, F., Foglini, F., Kruss, A., Ferrarin, C., Pizzeghello, N.M., Murri, C., Rossi, M., Bajo, M., Bellafiore, D., Campiani, E., 2017. High resolution multibeam and hydrodynamic datasets of tidal channels and inlets of the Venice Lagoon. Sci. Data 4, 170121. https://doi.org/10.1038/sdata.2017.121.

Madricardo, F., Foglini, F., Campiani, E., Grande, V., Catenacci, E., Petrizzo, A., Kruss, A., Toso, C., Trincardi, F., 2019. Assessing the human footprint on the sea-floor of coastal systems: the case of the Venice Lagoon, Italy. Sci. Rep. 9, 6615. https://doi.org/10.1038/s41598-019-43027-7.

Madricardo, F., Ghezzo, M., Nesto, N., Mc Kiver, W.J., Faussone, G.C., Fiorin, R., Riccato, F., Mackelworth, P.C., Basta, J., De Pascalis, F., Kruss, A., Petrizzo, A., Moschino, V., 2020. How to deal with seafloor marine litter: an overview of the state-of-the-art and future perspectives. Front. Mar. Sci. 7, 505134. https://doi.org/10.3389/fmars.2020.505134.

Madricardo, F., Bassani, M., D'Acunto, G., Calandriello, A., Foglini, F., 2021. New evidence of a Roman road in the Venice Lagoon (Italy) based on high resolution seafloor reconstruction. Sci. Rep. 11, 13985. https://doi.org/10.1038/s41598-021-92939-w.

Mai, L., Sun, X.-F., Xia, L.-L., Bao, L.-J., Liu, L.-Y., Zeng, E.Y., 2020. Global riverine plastic outflows. Environ. Sci. Technol. 54, 10049–10056. https://doi.org/10.1021/acs.est.0c02273.

Mai, L., Sun, X., Zeng, E.Y., 2023. Country-specific riverine contributions to marine plastic pollution. Sci. Total Environ. 874, 162552. https://doi.org/10.1016/j.scitotenv.2023.162552.

Maximenko, N., Corradi, P., Law, K.L., Van Sebille, E., Garaba, S.P., Lampitt, R.S., Galgani, F., Martinez-Vicente, V., Goddijn-Murphy, L., Veiga, J.M., Thompson, R.C., Maes, C., Moller, D., Löscher, C.R., Addamo, A.M., Lamson, M.R., Centurioni, L.R., Posth, N.R., Lumpkin, R., Vinci, M., Martins, A.M., Pieper, C.D., Isobe, A., Hanke, G., Edwards, M., Chubarenko, I.P., Rodriguez, E., Aliani, S., Arias, M., Asner, G.P., Brosich, A., Carlton, J.T., Chao, Y., Cook, A.-M., Cundy, A.B., Galloway, T.S., Giorgetti, A., Goni, G.J., Guichoux, Y., Haram, L.E., Hardesty, B.D., Holdsworth, N., Lebreton, L., Leslie, H.A., Macadam-Somer, I., Mace, T., Manuel, M., Marsh, R., Martinez, E., Mayor, D.J., Le Moigne, M., Molina Jack, M.E., Mowlem, M.C., Obbard, R.W., Pabortsava, K., Robberson, B., Rotaru, A.-E., Ruiz, G.M., Spedicato, M.T., Thiel, M., Turra, A., Wilcox, C., 2019. Toward the integrated marine debris observing system. Front. Mar. Sci. 6, 447. https://doi.org/10.3389/fmars.2019.00447.

Meijer, L.J., Van Emmerik, T., Van Der Ent, R., Schmidt, C., Lebreton, L., 2021. More than 1000 rivers account for 80% of global riverine plastic emissions into the ocean. Sci. Adv. 7, eaaz5803. https://doi.org/10.1126/sciadv.aaz5803.

Mel, R.A., Carniello, L., D'Alpaos, L., 2021. How long the Mo.S.E. barriers will be effective in protecting all urban settlements within the Venice Lagoon? The wind setup constraint. Coast. Eng. 168, 103923. https://doi.org/10.1016/j.coastaleng.2021.103923.

Mellink, Y.A., van Emmerik, T.H., Mani, T., 2024. Wind-and rain-driven macroplastic mobilization and transport on land. Sci. Rep. 14, 3898. https://doi.org/10.1038/s41598-024-53971-8.

Micheletti, C., Gottardo, S., Critto, A., Chiarato, S., Marcomini, A., 2011. Environmental quality of transitional waters: the lagoon of Venice case study. Environ. Int. 37, 31–41. https://doi.org/10.1016/j.envint.2010.06.009.

Ostoich, M., Ghezzo, M., Umgiesser, G., Zambon, M., Tomiato, L., Ingegneri, F., Mezzadri, G., 2018. Modelling as decision support for the localisation of submarine urban wastewater outfall: Venice lagoon (Italy) as a case study. Environ. Sci. Pollut. Res. 25, 34306–34318. https://doi.org/10.1007/s11356-018-3316-0.

Pascalis, F.D., Pérez-Ruzafa, A., Gilabert, J., Marcos, C., Umgiesser, G., 2012. Climate change response of the Mar Menor coastal lagoon (Spain) using a hydrodynamic finite element model. Estuar. Coast. Shelf Sci. 114, 118–129. https://doi.org/10.1016/j.ecss.2011.12.002.

Pascalis, F.D., Urbinati, E., Aalifar, A., Alcazar, L.A., Arpaia, L., Bajo, M., Barbanti, A., Barbariol, F., Bastianini, M., Bellafiore, D., Bellati, F., Benetazzo, A., Bologna, G., Bonaldo, D., Bongiorni, L., Braga, F., Brando, V.E., Brunetti, F., Caccavale, M., Camatti, E., Campostrini, P., Cantoni, C., Canu, D., Capotondi, L., Cassin, D., Castelli, G., Celussi, M., Correggiari, A., Cozzi, S., Dabalà, C., Davison, S., Fadini, A., Falcieri, F.M., Falcini, F., Ferrarin, C., Foglini, F., Gissi, E., Ghezzo, M., Grande, V., Guarneri, I., Lanzoni, A., Laurent, C., Lorenzetti, G., Madricardo, F., Manfè, G., Kiver, W.M., Menegon, S., Moschino, V., Nesto, N., Petrizzo, A., Pomaro, A., Ravaioli, M., Remia, A., Riminucci, F., Rosina, A., Rosati, G., Santoleri, R., Scarpa, G.M., Scroccaro, I., Stanghellini, G., Solidoro, C., Umgiesser, G., 2025. The DANUBIUS-RI supersite of Po delta and North Adriatic Lagoons: a living lab on transitional environments in the Adriatic Sea. Estuar. Coast. Shelf Sci. 324, 109453. https://doi.org/10.1016/j.ecss.2025.109453.

Pérez-Ruzafa, A., Fernández, A.I., Marcos, C., Gilabert, J., Quispe, J.I., García-Charton, J.A., 2005. Spatial and temporal variations of hydrological conditions, nutrients and chlorophyll a in a Mediterranean coastal lagoon (Mar Menor, Spain). Hydrobiologia 550, 11–27. https://doi.org/10.1007/s10750-005-4356-2.

Pesce, M., Critto, A., Torresan, S., Giubilato, E., Pizzol, L., Marcomini, A., 2019. Assessing uncertainty of hydrological and ecological parameters originating from the application of an ensemble of ten global-regional climate model projections in a coastal ecosystem of the lagoon of Venice, Italy. Ecol. Eng. 133, 121–136. https://doi.org/10.1016/j.ecoleng.2019.04.011.

Pinto, R.B., Van Emmerik, T.H.M., Duah, K., Van Der Ploeg, M., Uijlenhoet, R., 2024. Mismanaged plastic waste as a predictor for river plastic pollution. Sci. Total Environ. 951, 175463. https://doi.org/10.1016/j.scitotenv.2024.175463.

Puppin, A., Tognin, D., Ghinassi, M., Franceschinis, E., Realdon, N., Marani, M., D'Alpaos, A., 2024a. Spatial patterns of organic matter content in the surface soil of the salt marshes of the Venice Lagoon (Italy). Biogeosciences 21, 2937–2954. https://doi.org/10.5194/bg-21-2937-2024.

Puppin, A., Tognin, D., Paccagnella, M., Zancato, M., Ghinassi, M., D'Alpaos, C., Marani, M., D'Alpaos, A., 2024b. Blue carbon assessment in the salt marshes of the Venice Lagoon: dimensions, variability and influence of storm-surge regulation. Earth's Future 12, e2024EF004715. https://doi.org/10.1029/2024EF004715.

Regione del Veneto, 2022. Banca dati della Carta della Copertura del Suolo – aggiornamento 2020, Geoportale dei dati territoriali della Regione del Veneto. https://idt2.regione.veneto.it/idt/webgis/viewer?previewLayerId=13413. (Accessed December 2025).

Regione del Veneto, 2024. Limiti amministrativi poligonali dei comuni del Veneto, Geoportale dei dati territoriali della Regione del Veneto. https://idt2.regione.veneto.it/idt/webgis/viewer?previewLayerId=13977. (Accessed 8 December 2025).

Regione del Veneto – Sistema Statistico Regionale, 2025. Statistical database of the Veneto Region. https://statistica.regione.veneto.it/ENG/. (Accessed December 2025).

Roebroek, C.T.J., Laufkötter, C., González-Fernández, D., van Emmerik, T., 2022. The quest for the missing plastics: large uncertainties in river plastic export into the sea. Environ. Pollut. 312, 119948. https://doi.org/10.1016/j.envpol.2022.119948.

Rubinetti, S., Kuznetsov, I., Fofonova, V., Androsov, A., Gnesotto, M., Rubino, A., Zanchettin, D., 2023. Water mass transport changes through the Venice Lagoon inlets from projected sea-level changes under a climate warming scenario. Water 15, 3221. https://doi.org/10.3390/w15183221.

Safaie, A., Aalifar, A., Moallemi, M.A., 2026. The critical role of salinity in regulating eutrophication in Lake Urmia. J. Great Lakes Res., 102860 https://doi.org/10.1016/j.jglr.2026.102860.

Schmidt, C., Krauth, T., Wagner, S., 2017. Export of plastic debris by rivers into the sea. Environ. Sci. Technol. 51, 12246–12253. https://doi.org/10.1021/acs.est.7b02368.

Schreyers, L.J., van Emmerik, T.H.M., Bui, T.-K.L., van Thi, K.L., Vermeulen, B., Nguyen, H.-Q., Wallerstein, N., Uijlenhoet, R., van der Ploeg, M., 2024. River plastic transport affected by tidal dynamics. Hydrol. Earth Syst. Sci. 28, 589–610. https://doi.org/10.5194/hess-28-589-2024.

Segur, T., Sonke, J.E., 2025. Terrestrial and marine plastic pollution outlook in the Mediterranean region: a box-model approach based on OECD policy scenarios. Biogeosciences 22, 5139–5156. https://doi.org/10.5194/bg-22-5139-2025.

Strokal, M., Vriend, P., Bak, M.P., Kroeze, C., van Wijnen, J., van Emmerik, T., 2023. River export of macro- and microplastics to seas by sources worldwide. Nat. Commun. 14, 4842. https://doi.org/10.1038/s41467-023-40501-9.

Tarquini, S., Isola, I., Favalli, M., Mazzarini, F., Bisson, M., Pareschi, M.T., Boschi, E., 2007. TINITALY/01: a new triangular irregular network of Italy. Ann. Geophys. 50, 407–425. https://doi.org/10.4401/ag-4424.

Tasseron, P.F., van Emmerik, T.H.M., Vriend, P., Hauk, R., Alberti, F., Mellink, Y., van der Ploeg, M., 2024. Defining plastic pollution hotspots. Sci. Total Environ. 934, 173294. https://doi.org/10.1016/j.scitotenv.2024.173294.

Thompson, R.C., Courtene-Jones, W., Boucher, J., Pahl, S., Raubenheimer, K., Koelmans, A.A., 2024. Twenty years of microplastic pollution research—what have we learned? Science 386, eadl2746. https://doi.org/10.1126/science.adl2746.

Tognin, D., D'Alpaos, A., Marani, M., Carniello, L., 2021. Marsh resilience to sea-level rise reduced by storm-surge barriers in the Venice Lagoon. Nat. Geosci. 14, 906–911. https://doi.org/10.1038/s41561-021-00853-7.

Tommasini, L., Carniello, L., Ghinassi, M., Roner, M., D'Alpaos, A., 2019. Changes in the wind-wave field and related salt-marsh lateral erosion: inferences from the evolution of the Venice Lagoon in the last four centuries. Earth Surf. Process. Landf. 44, 1633–1646. https://doi.org/10.1002/esp.4599.

Umgiesser, G., Canu, D.M., Cucco, A., Solidoro, C., 2004. A finite element model for the Venice Lagoon. Development, set up, calibration and validation. J. Mar. Syst. 51, 123–145. https://doi.org/10.1016/j.jmarsys.2004.05.009.

Umgiesser, G., Ferrarin, C., Cucco, A., De Pascalis, F., Bellafiore, D., Ghezzo, M., Bajo, M., 2014. Comparative hydrodynamics of 10 Mediterranean lagoons by means of numerical modeling. J. Geophys. Res. Oceans 119, 2212–2226. https://doi.org/10.1002/2013JC009512.

Umgiesser, G., Zemlys, P., Erturk, A., Razinkova-Baziukas, A., Mėžinė, J., Ferrarin, C., 2016. Seasonal renewal time variability in the Curonian Lagoon caused by atmospheric and hydrographical forcing. Ocean Sci. 12, 391–402. https://doi.org/10.5194/os-12-391-2016.

Umgiesser, G., Ferrarin, C., Bajo, M., Bellafiore, D., Cucco, A., Pascalis, F.D., Ghezzo, M., McKiver, W., Arpaia, L., 2022. Hydrodynamic modelling in marginal and coastal seas — the case of the Adriatic Sea as a permanent laboratory for numerical approach. Ocean Model 179, 102123. https://doi.org/10.1016/j.ocemod.2022.102123.

van Emmerik, T., De Lange, S., Frings, R., Schreyers, L., Aalderink, H., Leusink, J., Begemann, F., Hamers, E., Hauk, R., Janssens, N., 2022. Hydrology as a driver of floating river plastic transport. Earth's Future 10, e2022EF002811. https://doi.org/10.1029/2022EF002811.

van Emmerik, T.H., Frings, R.M., Schreyers, L.J., Hauk, R., de Lange, S.I., Mellink, Y.A., 2023. River plastic transport and deposition amplified by extreme flood. Nat. Water 1, 514–522. https://doi.org/10.1038/s44221-023-00092-7.

Van Sebille, E., Aliani, S., Law, K.L., Maximenko, N., Alsina, J.M., Bagaev, A., Bergmann, M., Chapron, B., Chubarenko, I., Cózar, A., Delandmeter, P., Egger, M., Fox-Kemper, B., Garaba, S.P., Goddijn-Murphy, L., Hardesty, B.D., Hoffman, M.J., Isobe, A., Jongedijk, C.E., Kaandorp, M.L.A., Khatmullina, L., Koelmans, A.A., Kukulka, T., Laufkötter, C., Lebreton, L., Lobelle, D., Maes, C., Martinez-Vicente, V., Morales Maqueda, M.A., Poulain-Zarcos, M., Rodríguez, E., Ryan, P.G., Shanks, A.L., Shim, W.J., Suaria, G., Thiel, M., Van Den Bremer, T.S., Wichmann, D., 2020. The physical oceanography of the transport of floating marine debris. Environ. Res. Lett. 15, 023003. https://doi.org/10.1088/1748-9326/ab6d7d.

Verrelle, A., Glinton, M., Bazile, E., Le Moigne, P., Randriamampianina, R., Ridal, M., Berggren, L., Undén, P., Schimanke, S., Mladek, R., Soci, C., 2022. CERRA-Land sub-daily regional reanalysis data for Europe from 1984 to present, Copernicus Climate Change Service (C3S) Climate Data Store (CDS). 10.24381/cds.a7f3cd0b. (Accessed 15 December 2025).

Vianello, A., Boldrin, A., Guerriero, P., Moschino, V., Rella, R., Sturaro, A., Ros, L.D., 2013. Microplastic particles in sediments of Lagoon of Venice, Italy: first observations on occurrence, spatial patterns and identification. Estuar. Coast. Shelf Sci. 130, 54–61. https://doi.org/10.1016/j.ecss.2013.03.022.

Weiss, L., Estournel, C., Marsaleix, P., Mikolajczak, G., Constant, M., Ludwig, W., 2025. From source to sink: part 1—characterization and Lagrangian tracking of riverine microplastics in the Mediterranean Basin. Environ. Sci. Pollut. Res. 32, 10081–10104. https://doi.org/10.1007/s11356-024-34635-6.

Wickramarachchi, C., Niven, R.K., Kramer, M., 2025. Numerical plastic transport modelling in fluvial systems: review and formulation of boundary conditions. Water Res. 273, 122947. https://doi.org/10.1016/j.watres.2024.122947.

Willmott, C.J., 1981. On the validation of models. Phys. Geogr. 2, 184–194. https://doi.org/10.1080/02723646.1981.10642213.

Willmott, C.J., 1982. Some comments on the evaluation of model performance. Bull. Am. Meteorol. Soc. 63, 1309–1313. https://doi.org/10.1175/1520-0477(1982)063<1309:SCOTEO>2.0.CO;2.

Zanchettin, D., Bruni, S., Raicich, F., Lionello, P., Adloff, F., Androsov, A., Antonioli, F., Artale, V., Carminati, E., Ferrarin, C., Fofonova, V., Nicholls, R.J., Rubinetti, S., Rubino, A., Sannino, G., Spada, G., Thiéblemont, R., Tsimplis, M., Umgiesser, G., Vignudelli, S., Wöppelmann, G., Zerbini, S., 2021. Sea-level rise in Venice: historic and future trends (review article). Nat. Hazards Earth Syst. Sci. 21, 2643–2678. https://doi.org/10.5194/nhess-21-2643-2021.

Zirino, A., Elwany, H., Facca, C., Maicu', F., Neira, C., Mendoza, G., 2016. Nitrogen to phosphorus ratio in the Venice (Italy) Lagoon (2001–2010) and its relation to macroalgae. Mar. Chem. 180, 33–41. https://doi.org/10.1016/j.marchem.2016.01.002.

Zlateva, I., Ricker, M., Slabakova, V., Slavova, K., Doncheva, V., Staneva, J., Stanev, E., Popov, I., Gramcianinov, C., Raykov, V., 2024. Analysis of terrestrial and riverine sources of plastic litter contributing to plastic pollution in the Western Black Sea using a lagrangian particle tracking model. Mar. Pollut. Bull. 209, 117108. https://doi.org/10.1016/j.marpolbul.2024.117108.

Zuliani, A., Zaggia, L., Collavini, F., Zonta, R., 2005. Freshwater discharge from the drainage basin to the Venice Lagoon (Italy). Environ. Int. 31, 929–938. https://doi.org/10.1016/j.envint.2005.05.004.